NMRF/TR/04/2019

TECHNICAL REPORT

Implementation of Sub-Seasonal to Seasonal Forecast System with NCMRWF Global Coupled Model

Ankur Gupta, Ashis K. Mitra and E.N. Rajagopal

May 2019

National Centre for Medium Range Weather Forecasting
Ministry of Earth Sciences, Government of India
A-50, Sector-62, Noida-201 309, INDIA

Implementation of Sub-Seasonal to Seasonal Forecast System with NCMRWF Global Coupled Model

Ankur Gupta, Ashis K. Mitra and E.N. Rajagopal

May 2019

National Centre for Medium Range Weather Forecasting
Ministry of Earth Sciences
A-50, Sector 62, Noida-201309, INDIA

Ministry of Earth Sciences
National Centre for Medium Range Weather Forecasting
Document Control Data Sheet

1	Name of the Institute	National Centre for Medium Range Weather Forecasting
2	Document Number	NMRF/TR/04/2019
3	Date of publication	May 2019
4	Title of the document	Implementation of Sub-Seasonal to Seasonal Forecast System with NCMRWF Global Coupled Model
5	Type of Document	Technical Report
6	No. of pages & Figures	63 pages including 18 figures
7	Number of References	54
8	Author (S)	Ankur Gupta, Ashis K. Mitra and E.N. Rajagopal
9	Originating Unit	NCMRWF
10	Abstract	Prediction of anomalous weather episodes such as cold/heat waves, active/break phases of monsoon rainfall and convective activity over neighboring seas few weeks in advance is of considerable value for a country like India. Predictability of details of these transients' related events beyond medium range is very low. However, mean evolution of weather/climate averaged over space/time provides useful information about likely scenario in coming weeks to a season. As the evolution of space/time averaged anomalous features beyond few weeks is mainly dependent on the slowly varying boundary conditions like surface land/ocean temperatures, soil moisture, etc., it becomes necessary to use a coupled Atmosphere-Land-Ocean-Seaice model to capture the associated variability. This scientific basis helps to carry out prediction in sub-seasonal to seasonal (S2S) scale especially for the tropics. As part of the seamless modeling strategy at NCMRWF a fully coupled model configuration is implemented during June 2018 to form part of the extended range prediction (ERP) system producing up to four weeks of anomaly forecasts. On similar lines a seasonal prediction suite was also implemented and tested. This report documents the technical details of the implementation of both the ERP and seasonal suites on Mihir HPC. Details of the main component-models of the coupled system are given; the associated science configurations are also summarized briefly. The choice of remapping algorithm for exchange of fields at the coupling interface between component models has been described in detail. A set of hindcasts are carried out covering a period from 1993-2015. The twenty three year hindcasts initialized every week provides model climatology for computing week-by-week forecast anomalies up to four weeks. The hindcasts are initialized using ECMWF ERA-Interim reanalysis along with

		seasonally varying climatology of aerosols, ozone and soil moisture. The forecasts are initialized using real-time NCMRWF land-atmosphere and ocean-sea-ice analysis. The ERP suite documented here provides input for preparation of forecast charts of precipitation, circulation, sea-ice, and ocean variables shared with inter-ministerial institution on every Thursday. Sample forecasts of precipitation over Indian region, land/ocean surface temperature and seaice are shown. Following similar procedure the seasonal hindcast and anomaly forecast are also produced. The technical details of seasonal runs of up to 7 months of simulation carried out on Mihir HPC and some sample analysis are also described here.
11	Security classification	Non-Secure
12	Distribution	Unrestricted Distribution
13	Keywords	Coupled model, seamless modelling, monsoon, sea surface temperature, sea ice concentration, extended range prediction, seasonal forecast

Table of Contents

Abstract

Prediction of anomalous weather episodes such as cold/heatwaves, active/break phases of monsoon rainfall and convective activity over neighboring seas few weeks in advance is of considerable value for a country like India. Predictability of details of these transients' related events beyond medium range is very low. However, mean evolution of weather/climate averaged over space/time provides useful information about likely scenario in coming weeks to a season. As the evolution of space/time averaged anomalous features beyond few weeks is mainly dependent on the slowly varying boundary conditions like surface land/ocean temperatures, soil moisture, etc., it becomes necessary to use a coupled Atmosphere-Land-Ocean-Seaice model to capture the associated variability. This scientific basis helps to carry out prediction in sub-seasonal to seasonal (S2S) scale especially for the tropics. As part of the seamless modeling strategy at NCMRWF a fully coupled model configuration is implemented during June 2018 to form part of the extended range prediction (ERP) system producing up to four weeks of anomaly forecasts. On similar lines a seasonal prediction suite was also implemented and tested. This report documents the technical details of the implementation of both the ERP and seasonal suites on Mihir HPC. Details of the main component-models of the coupled system are given; the associated science configurations are also summarized briefly. The choice of remapping algorithm for exchange of fields at the coupling interface between component models has been described in detail. A set of hindcasts are carried out covering a period from 1993-2015. The twenty three year hindcasts initialized every week provides model climatology for computing week-by-week forecast anomalies up to four weeks. The hindcasts are initialized using ECMWF ERA-Interim reanalysis along with seasonally varying climatology of aerosols, ozone and soil moisture. The forecasts are initialized using real-time NCMRWF land-atmosphere and ocean-sea-ice analysis. The ERP suite documented here provides input for preparation of forecast charts of precipitation, circulation, sea-ice, and ocean variables shared with inter-ministerial institution on every Thursday. Sample forecasts of precipitation over Indian region, land/ocean surface temperature and seaice are shown. Following similar procedure the seasonal hindcast and anomaly forecast are also produced. The technical details of seasonal runs of up to 7 months of simulation carried out on Mihir HPC and some sample analysis are also described here.

1 Introduction

Weather in India goes through several regimes during a year. In summers, spells of continuous rainfall activity, occurrences of extreme rainfall events batter the Indian subcontinent. The non-occurrence of rainfall over an extended period during summer time directly impacts the seasonal mean rainfall and has been associated with some of the major draughts in the past decades. In pre- and post-monsoon season, the Bay of Bengal shows conditions favorable to genesis and intensification of tropical cyclones, several of which makes landfall mostly on the eastern coast of India. Associated with western disturbances, episodes of convective activity and sudden drop in temperatures are common in northern and north-east India during winter time. The developments in general circulation models in last 5-10 years have advanced the prediction skills of many such weather phenomena from 3 days to 5days, and even up to 7-10 days for many individual weather events(Bauer et al. 2015). However, weather was believed to be unpredictable at time scales longer than medium range (7-10-days). This would a gloomy situation especially in the context of summertime rainfall episodes in Indo-Gangetic plains and central India, where there is huge potential benefit to the agricultural community in knowing the likelihood of rainfall a few weeks in advance.

The atmospheric state was however considered to be unpredictable at longer time-scales due to non-linear response of flow instabilities to the uncertainties in initial conditions (Lorenz 1963). It was due to the theory of (Charney and Shukla 1981) that the importance of boundary conditions in the prediction of atmospheric state was established. They showed that a large part of tropical variability is driven by variability of boundary parameters such as sea surface temperatures, soil moisture, albedo and vegetation and planetary-scale flows, which vary slowly and are thus more predictable. The prediction at short to medium range has improved vastly since Epstein 1969first showed that by representing the uncertainties in initial conditions, probabilistic based forecasts can be made up to several days in advance. However, the extended range falls into a time scale in which the impacts of initial conditions are progressively diminished in General Circulation Models (GCMs) and response to variations in large scale boundary parameters is not realized. At seasonal scales, the predictability of Indian summer monsoon rainfall (ISMR) has been shown to come from slowly evolving modes of climate variability such as: El-Nino and Southern Oscillations (ENSO) (Shukla and Paolino 1983), Indian Ocean dipole (IOD) (Ashok et al. 2001), etc.

The rainfall in the core monsoon region is usually characterized by spells of sustained rainfall activity over a period of 2-3 weeks followed by a period of subdued and intermittent rainfall activity, together commonly known as active and break spells (Rajeevan et al. 2010). Rainfall over other parts of Indian mainland also shows enhanced intraseasonal variability during summer monsoon. With 30-40% of the daily rainfall variability being at intraseasonal time scales in tropics, the importance of extended/seasonal range forecasts during summer monsoon cannot be undermined (Goswami and Mohan 2001). The active and break spells are largely manifestation of intra-seasonal oscillations (ISOs) which shows a predominant northward propagation (Gadgil and Srinivasan 1990). Higher frequencies variability further modulates the day-to-day rainfall activity. The forecasts of rainfall beyond one week during summer monsoon thus depend on the correct simulation of the ISOs and the associated Intraseasonal Variability (ISV). The predictability of intraseasonal oscillations, which directly impacts the intraseasonal variability, has been studied extensively in the last decade (Abhilash et al. 2014; Lee et al. 2015; Y. Li et al. 2018). Recent studies with general circulation models shows that the predictability of intraseasonal oscillation depends on the correct simulation of the coupled ocean-atmospheric state at extended range (Demott et al. 2015). However, the atmosphere-only models show under-representation of ISOs in terms of their structure, amplitude and propagation (Klingaman and Woolnough 2014; Sharmila et al. 2013). Observations show significant phase dependency between precipitation and sea surface temperature (SSTs) anomalies with SSTs leading the precipitation anomalies by quadrature (Klingaman et al. 2008). Accurate representation of air-sea interactions have been showed to be important for the simulation of ISOs in the models; coupled models have shown better simulation compared to atmospheric-only models (Sharmila et al. 2013). Advances in model physics, resolution and representation of a dynamic lower boundary has resulted in improvement in representation of ISOs in GCMs (Li et al. 2016). This has allowed the advancement of skill of models up to 2-3 weeks for some tropical phenomenon, such as Madden-Julian Oscillations (MJOs) and Monsoon Intraseasonal Oscillations (MISO) (Abhilash et al. 2014; Lee et al. 2015), both of which have high variability at intraseasonal time scales. The prediction of ISOs has also improved in many current operational models (Liu et al. 2017). This provides a window of opportunity where dynamical models can be used to provide information about the state of these oscillations few weeks in advance (Brunet et al. 2010; Robertson et al. 2015; White et al. 2017).

Indian Meteorological Department (IMD) has been issuing the seasonal forecast of Indian summer monsoon rainfall (ISMR) since 1886. Since 1920s the statistical models have been used at IMD for issuing long range forecasts. The operational statistical models at IMD have undergone many recent developments (Rajeevan et al. 2004, 2007). In last many years, the importance of coupled dynamical models in seasonal forecasting has been increasingly recognized. While (Gadgil et al. 2005)discusses major problems of the statistical and dynamical models, several studies shows improved skill of coupled models in forecasting ISMR (Rajeevan et al. 2012). Different models may have different systematic biases; by designing a multimodel ensemble strategy some of the biases in models can be reduced. The multimode ensemble mean has been found to perform better than individual models.

As part of the United Kingdom Met Office (UKMO) Unified Model (UM) Partnership, NCMRWF has been continuously evolving towards a seamless modeling strategy and is currently implementing different configurations of the UKMO Unified Model (UM): global, regional and ensemble along with ocean and atmospheric data assimilation systems. Till recently, the realtime models at NCMRWF were based on land-atmospheric component only. However, including ocean-seaice component of the earth system is necessary for simulating the state of atmosphere at extended/seasonal range. During March 2017, a coupled modeling system was implemented at NCMRWF on Bhaskara, an IBM iDataPlex HPC, and was shown to capture the large scale atmospheric circulation and ocean-seaice state at up to 15 days of lead times(Gupta et al. 2019). During monsoon 2018, a coupled model configuration with both forecast and hindcast components was implemented at NCMRWF to form extended/seasonal range prediction system. The extended range prediction suite (ERPS) is running realtime on Mihir HPC and experimental forecast products are shared with meteorological community. This report outlines the essential components of extended/seasonal prediction systems along with the technical details of its implementation on Mihir, a Cray high-performance computing (HPC) supercomputer. The structure of the suite, initial conditions used in both re-forecasts (hindcast) and real-time forecasts, ancillary data used by the model, ensemble strategy, along with sample forecasts and preliminary analysis of the extended range forecast system has been described. The hindcast strategy has been discussed in detail.

In April 2019, first set of forecasts and 23 year hindcasts at seasonal scale were completed on Mihir HPC using April initial condition; June-September rainfall simulations from

these runs have been shown for demonstration purpose. Since prediction at sub-seasonal to seasonal scale follows some common scientific basis of averaging over space and time to compute the anomalies, the suites for both extended and seasonal systems follow similar software framework and related work flows. Technical details about the implementation of extended/seasonal forecast/hindcast suite and some preliminary results are also shown in this report.

2 Model Components

NCMRWF is a core member of United Kingdom Met Office Unified Model (UM) partnership and have several collaborative projects with members of the group. The member institutions jointly develop and reap the benefits from the latest developments in both the common technical infrastructure and improvements in science configurations. UM is evolving into a modeling system which is compatible to be seamlessly adopted for forecasting across time scales: from weather to seasonal to climate. The current coupled configuration implemented at NCMRWF include the UM as the atmospheric model and the Joint United Kingdom Land Environment Simulator (JULES) to represent land-surface. Nucleus for European Modeling of the Ocean (NEMO) is adopted as ocean model and seaice dynamics and thermodynamics are computed by subroutines in Los Alamos National Laboratory community-driven sea ice model (CICE).The land and atmospheric models are combined as single executable while ocean and seaice models are combined into separate executable. This choice of separating and combing different models stems from the development cycles of the coupled systems. For example, land-atmosphere modeling system followed the development cycles of the United Kingdom Met Office operational models. Similarly, patches to both NEMO and CICE models are applied to enable transfer of data within the ocean-seaice executable and also to enable coupling with the UM-JULES executable. Each of the model-components have ever-evolving science configuration associated with it. In this section, we briefly describe scientific configurations adopted here for each model component: Global Atmosphere 6.0 (GA6.0) and Global Land 6.0 (GL6.0)(Walters et al. 2017), Global Ocean 5.0 (GO5.0) (Megann et al. 2014) and Global Sea Ice 6.0 (GSI6.0)(Rae et al. 2015). Together these are known as Global Coupled configuration and we adopt GC2 version of it. A detailed description of scientific configuration adopted here is given in (Gupta et al. 2019). GC2 shows improvements over earlier configuration particularly for

simulation of temperature and climate modes like El-Nino and Southern Oscillations (ENSO) and the North Atlantic Oscillation (NAO) (Williams et al. 2015).

2.1 The Atmospheric Model

The UM is a non-hydrostatic, full compressible deep atmospheric model discretized on Arakawa C-grid in horizontal and uses Charney-Phillips vertical staggering having semi-implicit semi-Lagrangian scheme for time-stepping. Terrain-following hybrid-height coordinate in model has maximum height of 85 km with 85 levels. Horizontal model resolution is defined as N216 which is a regular grid with grid size ~65 in mid-latitudes. The dynamical core of the model called ENDGame (Even Newer Dynamics for General atmospheric modeling of the environment) is fully documented in (Wood et al. 2014). The nested approach of ENDGame has improved stability of the model which allows implementation of near semi-implicit numerical scheme which is more accurate than earlier dynamical core called New Dynamics. Improved stability also allowed discontinuation of polar filtering, making the code more scalable. Physical processes are represented by set of parameterization schemes. The radiation scheme is based on (Edwards and Slingo 1996). A modified version of mass flux based convection scheme of (Gregory and Rowntree 1990) is adopted. Unresolved turbulent motions in both free troposphere and boundary layer are represented using scheme based on (Lock et al. 2000). In addition, model has extensive parameterization schemes to represent large-scale precipitation (Wilson and Ballard 1999), prognostic cloud fraction and prognostic condensate (PC2) (Wilson et al. 2008), drag due to sub-grid orography (Lott and Miller 1997) and effects of gravity waves (Scaife et al. 2002).

2.2 The Land-surface Model

JULES, described fully in (Best et al. 2011), is a community land surface model developed by United Kingdom researchers and Centre for Ecology and Hydrology available freely for non-commercial use. Here a configuration GL 6.0 is adopted; the horizontal grid is same as that of atmospheric model with 4 vertical levels. 9 types of vegetations are represented in each grid point by tiles of different properties. The surface similarity functions are used to parameterize surface heat and momentum fluxes. GL 6.0 also includes a hydrological model to represent rainfall-runoff relationship and sub-surface water flow. The excess runoff is routed via river-routing routines.

2.3 The Ocean Model

NEMO ocean model used in current coupled configuration is at eddy-permitting resolution of $1/4^o$ having a tripolar orthogonal curvilinear grid, ORCA025, in horizontal and 75 vertical levels reaching a depth of 6000 m with higher resolution of 1 m in the upper ocean. The spatial discretization is based on centered second-order finite difference approximation. The generalized Arakawa C-grid is used to represent the variables in which the scalars are located at cell's center and vectors are located at the center of faces of the cell. The model solves the prognostic equations in their vector invariant form in which Coriolis and advection terms are decomposed into vorticity, kinetic energy and vertical advection terms. Other forces include horizontal and surface pressure gradients, and contributions from lateral and vertical diffusion. For diffusive terms, a backward (or implicit) time differencing scheme is used. Non-diffusive forcings are solved using well known leapfrog time-differencing scheme of (Mesinger and Arakawa 1976) with some modifications. Surface layer height is a diagnostic variable and is computed by integrating the linear surface kinematic condition. Explicit filtering of fast gravity waves is implemented to allow reasonable time step for model integrations. Diapycnal mixing is parameterized using a modified version of (Gaspar et al. 1990) turbulent kinetic energy scheme. The effect of energy transfer from barotropic tides to internal tides and internal tide breaking due to rough topography is parameterized based on (Simmons et al. 2004), with enhanced tidal dissipation efficiency in the region of Indonesian Throughflow to account for trapped internal waves in the Indonesian Archipelago. An advective and diffusive bottom boundary layer scheme based on (Beckmann and Döscher 1997) is also included.

2.4 The SeaiceModel

The seaice surface temperatures and surface fluxes needs to dynamically evolve in a coupled model. Traditionally, UKMO coupled models are coupled every 24-hour. This prevents the diurnal cycle of key variables at the atmosphere-seaice interface to be resolved. Thus in HadGEM family of models, the sea ice computations related to seaice thermodynamics is split between atmosphere and ocean(McLaren et al. 2006). The UM-JULES model computes atmosphere-ice radiative and heat fluxes, the diffusive heat flux through the ice, and the ice surface temperature. Unlike ocean treatment of solar heat fluxes, where solar fluxes are partitioned into penetrative and non-penetrative fluxes, atmospheric computation of surface

fluxes over seaice assume all solar fluxes to be absorbed and thus none passes through ice to the ocean. To allow such sub-daily treatment of surface fluxes over seaice when coupling frequency is sub-optimal to resolve diurnal variability, the GC2 uses a modified version of CICE. Note this is not the issue with standalone CICE as it can update surface fluxes depending on forcing data available. The CICE code used here implements zero-layer thermodynamics to calculate the growth and melt of the sea ice, with one layer of snow and one layer of ice. The land-atmosphere model also computes seaice albedo as a function of temperature, snow cover and melt ponds. The surface heat flux, latent heat flux, and conductive flux through ice determines the growth or melt rates of seaice. The heat is also exchanged between ocean and seaice at the bottom surface of seaice and also when frazil ice forms in ocean. These are then linearly remapped to transport the ice between thickness categories. Five categories of seaice based on thickness are included in GO5.0 with elastic-viscous-plastic ice dynamics of (Hunke and Dukowicz 1997) and energy-conserving thermodynamics of (Bitz and Lipscomb 1999). Note that CICE has multi-layer thermodynamics which cannot be used here as seaice surface temperatures and the conductive heat fluxes into seaice are computed by atmosphere-land model and not seaice model for the reasons specified above. This dependency on UM for computing seaice surface temperatures and heat fluxes through seaice will not be necessary in sub-daily coupling frequency and thus later versions of the coupled configurations are expected to use multilayer seaice thermodynamics.

3 Remapping algorithm for exchange of fields at coupling interface

One of the advantages of coupling different models is that it allows the forcings and boundary conditions at the model interfaces to be updated during simulation instead of being represented as static fields. To exchange fields between different component models, a remapping algorithm with desired accuracy is required when the component models are defined on different grids. The interpolation of fields from source to destination model grids thus allows the fields computed in source model to be made available to the destination model. However, interpolation of fields on discrete grids is susceptible to numerical errors which could amplify during longer runs. Component models are designed to conserve mass and energy within a known range of accuracy. However, errors in fields received the coupling interface can introduce mass and energy imbalances in the component models. Thus, heat, momentum and freshwater fluxes need to be conserved for the stability of long runs. Here, we use first order conservative

remapping for all scalar fields exchanged from atmosphere to ocean and second order conservative remapping for all scalar fields exchanged from ocean to atmosphere. Because the second order conservative remapping can introduce over- and under-shoots near sharp gradients in the source fields, such a scheme cannot be used for atmospheric variables such as shortwave fluxes, precipitation, runoff, wind speed etc. which are defined to be positive numbers. The remapping of vector fields, such as ocean currents and wind stress, is done by bilinear remapping due to technical difficulties in interpolating vector grids between arbitrary girds(Hewitt et al. 2011). The lack of conservation of momentum during remapping has not been found to create serious issues during climate simulations using earlier versions of this coupled modeling framework(Hewitt et al. 2011). SCRIP software is used for creating remapping files. It needs locations of center and corners of each grid point in input and output grids, the remapping weights are generated using user defined algorithm (bilinear, conservative etc.). The area of each cell is also computed for conservative remapping. There are 6-different grids in current implementation; these are U, V, and T, each for land-atmosphere ocean-seaice component models. Creating remapping weights using SCRIP takes several minutes and thus a performance penalty. Thus, while OASIS3 coupler used here can generate online weights during runtime, remapping weights generated apriori are used here.

OASIS3 also have several routines for pre-processing of fields, such as but not limited to time averaging over the coupling frequency. Since the ocean grid is curvilinear, the vectors are rotated within the ocean model before sending to atmosphere and after receiving fields from atmosphere. The coupling sequence is fixed apriori to avoid any deadlock in model simulation, such as when models involved in coupling waits for the exchange of fields at the same execution time. The models are initialized using their respective dumps, coupling fields are then exchanged before model simulation, and then each of component models run up to coupling period. The simulation continues beyond each coupling event only after the fields are thus exchanged. Coupling frequency is set to every 3 hours. A full list of coupling fields along with choice of remapping algorithm and relevant preprocessing for each field is provided in(Gupta et al. 2019).

4 Initialization of Forecasts and Hindcasts

Each of the component models: atmosphere, land, ocean, and seaice, are initialized from respective startdumps. The initialization strategies are different for the re-forecasts and forecasts,

and have been described below. Choices for initialization of boundary conditions are described in detail for both hindcasts and forecasts particularly for amount of snow, soil temperature, soil moisture, surface temperature (over land, ocean, snow and seaice) and seaice concentration.

4.1 Atmosphere Initialization

A large number of fields are required to be initialized as needed by dynamic and physical parameterization routines in UM. A complete list of initialized variables in both forecasts and hindcasts is provided in Appendix A. The forecasts are initialized from NCMRWF atmospheric analysis which is produced operationally using a hybrid-4DVar data assimilation system(Kumar et al. 2018). A list of all variables initialized from stardump is provided in Table A.1.The assimilation system uses a large number of observations and model background to optimally estimate dynamically consistent state of atmosphere by minimizing the departure of the forecasts from observations over the assimilation window using weighing functions based on observations and model background error covariance matrices. Hybrid-4DVar is an advanced data assimilation system which is coupled to the ensemble forecasting system at NCMRWF by combining errors estimated from ensemble of daily forecasts with climatological model background errors to compute the error covariance matrix. However, a large number of variables are left undefined as the estimation of their current values is either not available or not of interest. Many such important variables, particularly those related to boundary parameters and aerosols concentrations, are initialized from the climatology and some are updated at regular intervals during model simulations. Table A.3 lists all such variables along with the name and relative paths of ancillary files from where such variables are read during reconfiguration and forecast step of the coupled-model suite. (Walters et al. 2017) describe the source of these atmospheric ancillary fields. These files can be broadly categorized into those representing a) land parameters: orography, mean and standard deviation of the topography, land mask, land fraction and albedo); b) vegetation parameters: fraction of surface types, leaf area index, canopy height; c) soil parameters: saturated soil conductivity, volumetric soil moisture at saturation etc.; d) river parameters: river sequence, direction and storage; e) aerosols: sulphate (accumulation, aitken, and dissolved modes), sea salt (film and jet modes), dust (6-types), black carbon (fresh and aged); e) Emissions: from biogenic sources, fresh, aged, in-cloud modes from biomass burning and combustion of fossil fuel (organic carbon); and g) ozone. Other initialized variables

are either set to zero, a constant, a missing value or computed from other fields in the startdump. A list of all such fields is provided in

Table A.**4** to

Table A.**11**.

The hindcasts are initialized using ECMWF ERA-Interim reanalysis(Dee et al. 2011). The ERA-Interim reanalysis used here is at 60 levels and at 0.75 degree resolution. It is reconfigured to L85 vertical grid (reaching 85 km) and N216 regular grid for running atmospheric model. As discuss above a large number of variables are initialized from operational startdumps for the forecasts. However, only a small subset of variables is initialized from reconfigured ECMWF analysis (Table 1). The remaining fields are either set to zero or some constant values. The details of each of such variable and method used to initialize them are provided in Table A.9, Table A. **10** &

Table A.**11** in Appendix A.2. It is useful to note that the hindcasts use exactly same ancillary data as used by the forecasts. Further many of other variables are initialized consistently between forecasts and hindcasts and listed in Table A.3 to Table A.8 in Appendix A.1.

Table 1: Variables from ECMWF reanalysis used for initializing the hindcasts

Number of Levels	Stash Code	Description
1	30	land mask (no halo) (land=true)
1	33	orography (/strat lower bc)
1	24	surface temperature after timestep
1	409	surface pressure after timestep
60	2	u compnt of wind after timestep
60	3	v compnt of wind after timestep
60	16004	temperature on theta levels
60	10	specific humidity after timestep
4	20	deep soil temp after timestep
1	23	snow amount over land aft tstp kg/m2
60	254	qcl after timestep
60	12	qcf after timestep

4.2 Land-surface Initialization

For the realtime coupled runs up to 15-days, soil temperature and soil moisture are initialized from land-surface analysis from simplified extended Kalman filter land-surface data assimilation system which uses ASCAT soil wetness and other surface temperature and humidity observations. However, soil moisture from the realtime analysis cannot be used in the current extended range prediction system, as the soil moisture climatology from UKMO based assimilation system differs significantly from the ERA-Interim (Maclachlan et al. 2015). This prevents use of soil moisture from ERA-Interim in hindcast-initialization and use of NCMRWF soil moisture analysis for the forecast system. Thus a soil moisture monthly climatology developed by UKMO is used to initialize both the forecasts and hindcasts. Snow-depth and soil temperature are taken respectively from satellite estimates and NWP analysis for the forecasts and ERA-Interim for the hindcasts.

4.3 Ocean and Seaice Initialization

The ocean and sea-ice initial conditions are produced at NCMRWF (Momin et al., 2019)using NEMOVAR which is an incremental 3D-Var data assimilation system using first guess at approximate time (FGAT) as background field(Waters et al. 2015). The system assimilates both satellite and *in situ* observations of SST, sea-level anomaly, sub-surface temperature and salinity profiles, and satellite observations of sea-ice concentrations over 1-day assimilation cycle. The ocean-sea-ice model is same in both the data assimilation system and forecast model. The startdumps for the hindcast initialization are taken from GloSea Ocean and Sea Ice Analysis, which is from the same system as used in the realtime ocean data assimilation system but with ERA-Interim forcings.

5 Extended Range Prediction Suite

All the tasks covering the complete work flow: compiling the component model executables, retrieving startdumps, scheduling hindcasts, reconfiguration of the startdumps, running coupled model, post-processing, archiving and housekeeping are combined into a single suite. The suite is configured into two modes: hindcasts and forecasts. The two modes differ on the logistics of preparing a set of initial conditions and scheduling different startdates. More thought is to be

given while designing the hindcasts schedule, as the work-load assigned to each cycle depends on choices such as number of hindcast years and number of perturbed members. Common to each mode is a coupled model with three executables:

1) OASIS: the coupler which calls component models, prepares and exchanges data at the executable interfaces.
2) UM-JULES: land-atmosphere model compiled as a single executable.
3) NEMO-CICE: ocean-seaice model compiled as a single executable

It should be noted that the data is exchanged using subroutine arguments of accessing shared data arrays between component models of each executable. The coupling fields are exchanged by specific routines maintained under OASIS libraries. The coupled model used for simulation is same in both modes, with the exception of initialization and storing of simulated fields. It can be envisaged that the fields of interest and their output frequency could be different for hindcasts and forecasts. The desired output fields, domain and frequency from model runs can be changed using the STASH processing in UM-JULES executable, XML based namelist for NEMO, and FORTRAN based namelist for CICE.

5.1 Software for workflow execution: ROSE, CYLC and FCMs

Here we use a combination of software ROSE, CYLC and FCM to execute the complete workflow as a single suite. Combining all components of the complex workflow into a suite of interdependent tasks allows consistent maintenance of the ported configuration. Further, the structure of ROSE-CYLC allows inheritance of a parent suite, and also importing components from different suites if required to achieve desired work-flow.

The models source code, coupling specific branches and configuration files containing compilation flags are managed and component models are compiled using Perl-based Flexible Configuration Manager (FCM). It imposes certain coding standards which allow automatic generation of dependencies for compiling numerical codes. The UM, JULES, NEMO and CICE models are mostly FORTRAN codes, and depend on FORTRAN based namelist to control large number of runtime variables. These are run-length, time-stepping, MPI decomposition, parameters in several physical parameterization and numerical schemes, etc. Variables such as run-length, resubmission intervals etc. are common to all coupled-executables. Thus a common way of controlling these runtime variables is required. Python based software called ROSE

fulfills this requirement by providing control over runtime variables. Modules within ROSE such as pre-scripting, post-scripting, env-scripting, etc. allows separation of environment into different compartments which are designed to provide both common environment across sites and site-specific machine and porting environment to individual porting sites. Ability to inherit parent-tasks allows a user to define common environment while maintaining modified task environment facilitation porting across sites.

The current suite is highly complex with a range of interdependent tasks (see below). The task of defining interdependencies could become cumbersome and prone to human errors. Again a Python based meta-scheduler called CYLC is used here for automatic generation of dependencies for interdependent tasks. CYLC also defines the job submission environment and schedule for each task based on generated dependencies. That is it checks the status of dependencies before preparing each task for submission. In current implementation CYLC uses Portable Batch Scheduler (PBS) for this purpose.

5.2 Workflow and individual tasks

The current suite consists of several tasks. A simplified workflow is presented in Figure 1 which also shows the interdependency of tasks. Each of the tasks is described below:

1) **install_cold**: This is a relatively simple task which links all executables, static files needed for model runs.
2) **gs_start, gsfc_start, and gshc_start**: These tasks act as gatekeeper to further tasks down in dependency chart. These are useful when a range of cycles are triggered and the 'gatekeepers' allow further execution of the workflow based on whether the cycles are dependent on each other, or if a dependent cycle has finished execution. These tasks can also be defined to wait for a given wall-clock time or the availability of startdumps which are usually the end-product of other suites.
3) **gshc_init_control_file**: This is a key task which allocates each startdate for each of the perturbed member to a cycle based on specified number of members intended to be finished per cycle. It stores this information in a control file which is used by all subsequent tasks in the hindcasts workflow. The forecast workflow doesn't require this task, as all members starting from a given startdate are assigned to the cycle defined by the forecast startdate.

4) **gshc_register_member_m1**: This task is again a key component of hindcast workflow. From all the members in the control file it registers only those members which are assigned for the current cycle. On the success of registering a given hindcast year and perturbed member, the further tasks of reconfiguration and model runs can be triggered.
5) **gsfc_get_analysis**: This task links the realtime UM and NEMO startdumps produced on Mihir HPC. The ocean restart files on 192 processors are combined to form a single startdump.
6) **gshc_get_analysis**: This task retrieves the ECMWF ERA-Interim and copies the ocean and seaice startdumps into the cylc-run directory of the suite. The ocean startdumps are available as a single dump, and thus the task of combining output from different processors into a single dump is skipped in the hindcasts mode.
7) **gsfc_recon and gshc_recon**: Each of these tasks reconfigure the atmospheric dumps to the horizontal and vertical resolution of the coupled model. The hindcast and forecast reconfiguration differs to great extent. The hindcasts uses ERA-Interim grib files for 12 fields specified in Table 1, rest of the fields are either set to constants or initialized from ancillary files. The forecasts use realtime land-atmospheric dumps from Hybrid-4DVar data assimilation system at NCMRWF. Similarly, the ocean-seaice dumps are from the GloSea5 Ocean and Sea Ice Analysis for the hindcasts and the ocean analysis from 3D-Var assimilation system using first guess at approximate time (FGAT) for the realtime forecasts.
8) **gsfc_model_m1_s01** and **gshc_model_m1_s01**: These are respectively the main simulation tasks for forecasts and hindcasts. Each of them run a coupled model which is a combination of three executables running concurrently with a predefined sequence of exchange of fields at coupling intervals. 3-hourly coupling is implemented here. The component models have been described in section 2 and details of fields exchanged at the coupling interface have been described in Section3. The following command is used to run three executables concurrently on Cray HPC:aprun -cc cpu -n 32 -N 32 -S 16 -d 1 -j 1 oasis3 : -cc cpu -n 1200 -S 16 -d 1 -j 1 toyatm : -cc cpu -n 128 -S 16 -d 1 -j 1 env MPICH_RANK_REORDER=3 toyocewhere ‘oasis3’ is the name of the coupler executable and ‘toyatm’ and ‘toyoce’ are the name of the component model executables

expected by the coupler. These are linked to a centrally compiled executables and available for both forecast and hindcast modes.

9) **gsfc_model_m1_failed**: The coupled model is triggered up to a maximum of three times if a given submission fails. The workflow is allowed to proceed if a given member fails to finish even at the third attempt. This is important for the hindcasts where failure due to a single member can halt the execution of complete sequence determined in gshc_init_control_file task.
10) **gsfc_post_model_m1_s01**: The atmospheric output variables are moved from 'work' to 'cycle' directory.
11) **gsfc_ncdf_proc_m1_s01**: Ocean model creates output files according to the grid-type and frequency intervals. Each of the 128 ocean processors creates output files over the domain it covers. A utility called rebuild_nemo is used to combine these output file from different processors into a single file defined over global domain. All files having different grid-type or frequency interval from a single forecast or hindcast are processed in parallel processes on a single processor to achieve faster processing times per cycle. However, number of variables which can be processed in parallel on a given processor is limited by the memory required for combining one global variable. Peak memory usage during processing of each forecast (hindcast) output is 25% (12.5%) of total memory on a single MAMU node. Thus 4(8) of such output processing can be executed simultaneously on a single node. A dedicated MAMU node is required for processing of such memory intensive jobs with submission of jobs scheduled to match the memory available on a MAMU node. During realtime operations, an inadvertent additional job submission on the HPC system can stop the execution of rebuild_nemo. Given the limited availability of dedicated MAMU nodes, the rebuild_nemo is re-designed for execution on compute nodes. The limitation of single-job execution posed by CRAY compute nodes is mitigated by use of multiple nodes for post-processing when workflow necessitates processing more than one forecast or hindcast.
12) **gsfc_process_m1_s01, gsfc_archive_m1_s01, and housekeep**: Process and archive tasks are kept as dummy tasks to allow any future processing and archiving of data. Housekeeping tasks removes temporary files generated during the suite, which are no longer required: combined ocean startdumps, atmospheric reconfigured startdumps.

Directories such as log, work and cycle older than 7-days are also removed.

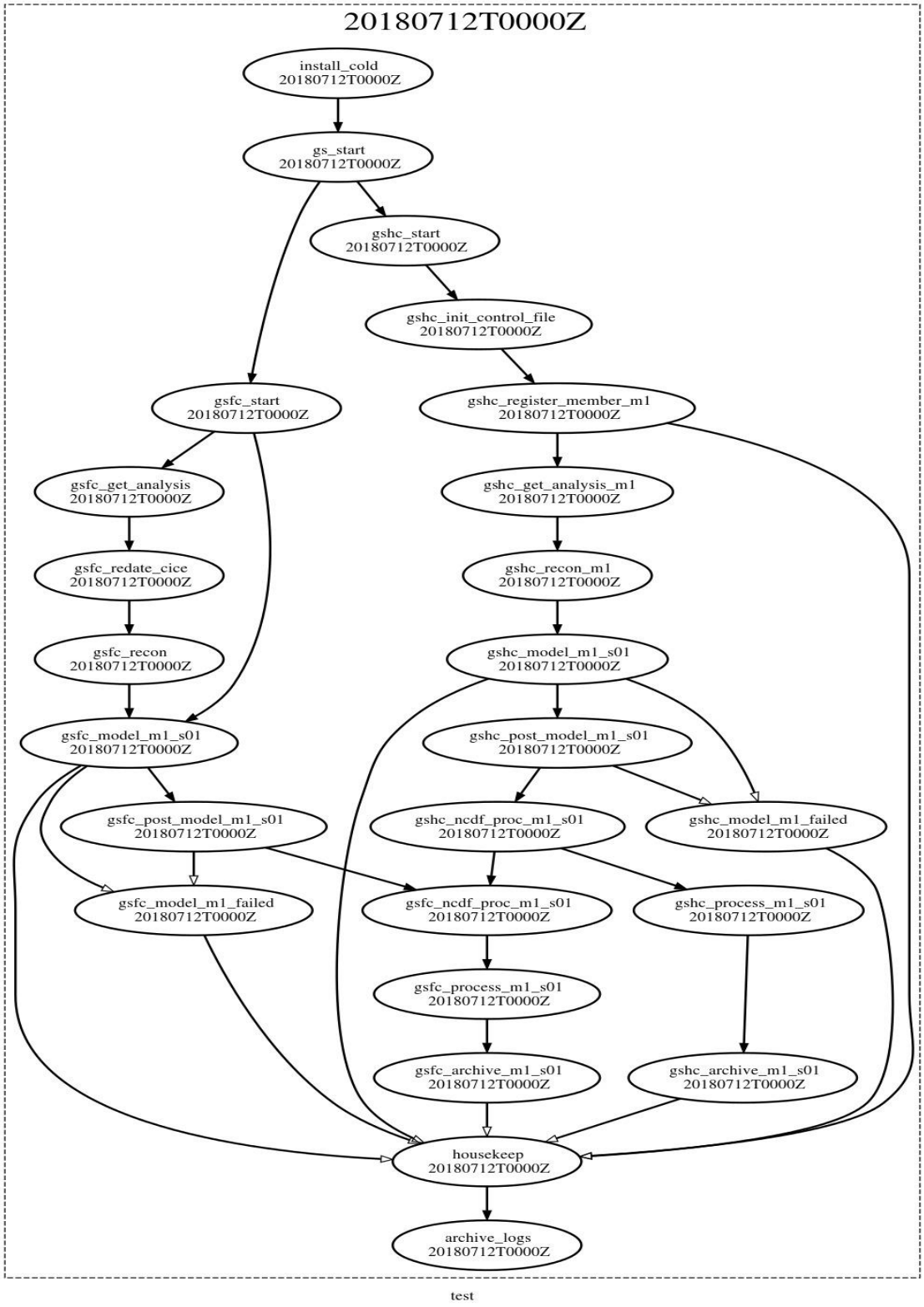

Figure 1: A simplified workflow for each cycle

5.3 HPC Resource Usage

Here we describe the daily HPC resource usage needed to complete a set of both hindcasts and forecasts needed to produce up to 4 weeks of forecasts and anomalies by every Thursday. Two types of job queues are available on Mihir HPC based on the access to compute nodes or MAMU nodes. Unlike compute nodes, MAMU nodes allow multiple jobs to be run concurrently. Tasks are assigned to a particular queue type after careful consideration of resource availability. Only the coupled model is run on CRAY compute nodes which are optimized for parallel processing. All other tasks such as reconfiguration, preprocessing, post-processing and housekeeping are done on background or MAMU nodes. Since MAMU nodes allow multiple executables to be run simultaneously, all serial jobs, preprocessing and post-processing tasks are configured to run on it, except for ocean post-processing for the reasons discussed in Section 5.2. The key submission directives for most resource intensive tasks are summarized in Table 2. The daily resource usage is depicted in Figure 2 for 7 hindcast and 2 forecast members to maintain the operational load balancing discussed in Section 5.4. Note, due to the parallel design of the work flow, wall-clock time taken by complete processing of single forecast/hindcast is same as in Figure 2.

Of the tasks shown in Figure 1, most resource intensive tasks are: gshc_model_m1_s01 and gsfc_model_m1_s01. These tasks prepare and submit the coupled model for 36 days of simulation on CRAY compute nodes with following MPI configuration.

aprun-cc cpu -n 32 -N 32 -S 16 -d 1 -j 1 oasis3 : -cc cpu -n 224 -S 16 -d 1 -j 1 toyatm : -cc cpu -n 128 -S 16 -d 1 -j 1 env MPICH_RANK_REORDER=3 toyoce

That is 32 processors are needed for OASIS coupler, while UM-JULES and NEMO-CICE uses 224 and 128 processors respectively with following domain decomposition:

UM_ATM_NPROCX="8", UM_ATM_NPROCY="28"

NEMO_OCN_NPROCX="8", NEMO_OCN_NPROCY="16"

With 32 or 36 processors used from each node, the node requirement for the coupled-task is 12 nodes.

The second most resource intensive task is from NCDF family. While gshc_ncdf_proc_m1_s01 takes only 40 minutes on a single processor on compute node, the

gsfc_ncdf_proc_m1_s01 takes twice as much. Only monthly mean forecasts are desired from the hindcasts. However, fields such as 3-hourly fluxes, 12-hourly and daily-mean 3-D temperature, salinity and several seaice parameters are stored for the first seven days of simulation in forecasts. Combined size of these additional ocean-seaice parameters in forecast mode is ~50 Gb which is substantial given the monthly output files from hindcast have combined size of less than 5 Gb. As NEMO output is produced separately on of the 128 processors, processing of these additional variables in the forecast mode takes another 40 minutes of processor time. Ideally, the post processing of all 9 members per day could be triggered simultaneously on MAMU nodes. However, for the reasons discussed in Section 5.2 NCDF tasks are configured such that each task used one compute node.

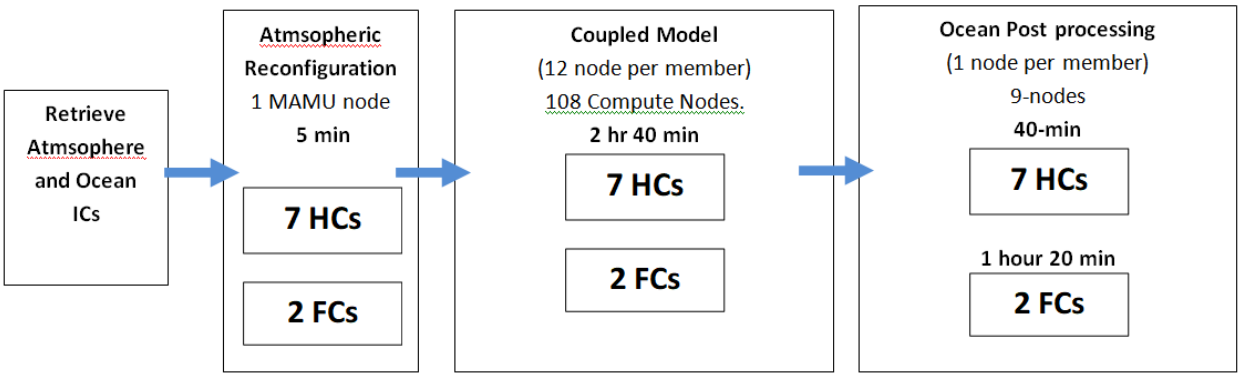

Figure 2: Daily Resource Usage for production of 2 forecast (FC) and 2 hindcast (HC) members.

Table 2: Key submission directives for most resource intensive tasks

gsfc_model_m1_s01, gshc_model_m1_s01
#PBS -q NCMRWF1
#PBS -l select=12:ncpus=32:vntype=cray_compute -l place=scatter
#PBS -l walltime=10800
gsfc_ncdf_proc_m1_s01, gshc_ncdf_proc_m1_s01
#PBS -q NCMRWF1
#PBS -l select=1:ncpus=36:vntype=cray_compute -l place=scatter
#PBS -l walltime=7200
gsfc_recon
PBS -q serial1
#PBS -l select=1:ncpus=1:vntype=cray_mamu
#PBS -l walltime=1200

The reconfiguration task during the forecast mode (gsfc_recon) takes twice the time than during the hindcast mode (gshc_recon) although output grid of N216 is same in both modes. The difference comes mainly due to extra time taken by reconfiguration task while reading the high resolution dump during the forecasts mode. The hindcasts use ECMWF fields in GRIB format at 0.75 x 0.75 degree resolution, which is much coarser resolution as compared with N1028 of atmospheric dump used in the forecast mode. Nevertheless, at 2.5 minutes for hindcast and 5 minutes for forecast the reconfiguration tasks consume only nominal HPC resources. During the extended range suite execution, many hindcast members are run concurrently. For each member a new reconfiguration task is spawned and submitted to the PBS. The waiting time in PBS is avoided for reconfiguration tasks by configuring the job submission module of CYLC for this task for MAMU nodes, where multiple jobs can be submitted simultaneously. Specifically, this is done by PBS directives given in Table 2, loading the cray-snplauncher module and using

/opt/cray/pe/snplauncher/7.6.3/bin/mpiexec to run the executable.

5.4 Operational Weekly Load Balancing

A particular feature of current implementation is that the hindcasts component is run concurrently with the forecast component. This allows the model and its scientific components to be consistent in forecasts and hindcasts. This also allows better load balancing as computational expensive job of producing hindcasts can be spread over a year; and a scientifically acceptable configuration can be immediately implemented for realtime operations from a given startdate without aprior production of all hindcasts. Any future upgrade in the system can thus be seamlessly adopted by prioritizing the production of hindcasts nearest to the forecasts initialization dates. To compute weekly forecast anomalies model climatological forecast must be known based on appropriate initial condition as discussed earlier. For this purpose, twenty three years of hindcasts (1993-2015) are to be carried out each week for a given startdate. Depending on the spread desired in the hindcasts, total number of hindcasts in a given week is: n*N, where n is the number of perturbed members and N is number of hindcast years. For a 2-member hindcast this means that 46 hindcasts are to be carried out in a week. Thus in realtime implementation 7 hindcast members are run each day except for Wednesday when only 4 members are run. Hindcasts for the lower perturbation number are scheduled earlier that those with higher perturbation number. This allows the hindcasts for all years to be finished on Sunday

for the first member. Note the weekly load balancing shown in Figure 3 is designed to complete 2 members per each hindcast and forecast startdate. The shaded boxes are optional load balancing to allow 3 members for each forecast startdate with forecasts initialized every day of the week. Currently, forecasts are initialized only Monday, Tuesday and Wednesday of each week. Additional 4-member hindcasts set are achieved by running the suite in hindcast mode separately from the realtime implementation. This allows increasing the sample size of hindcasts as required to assess the skill of the model with a given statistical significance.

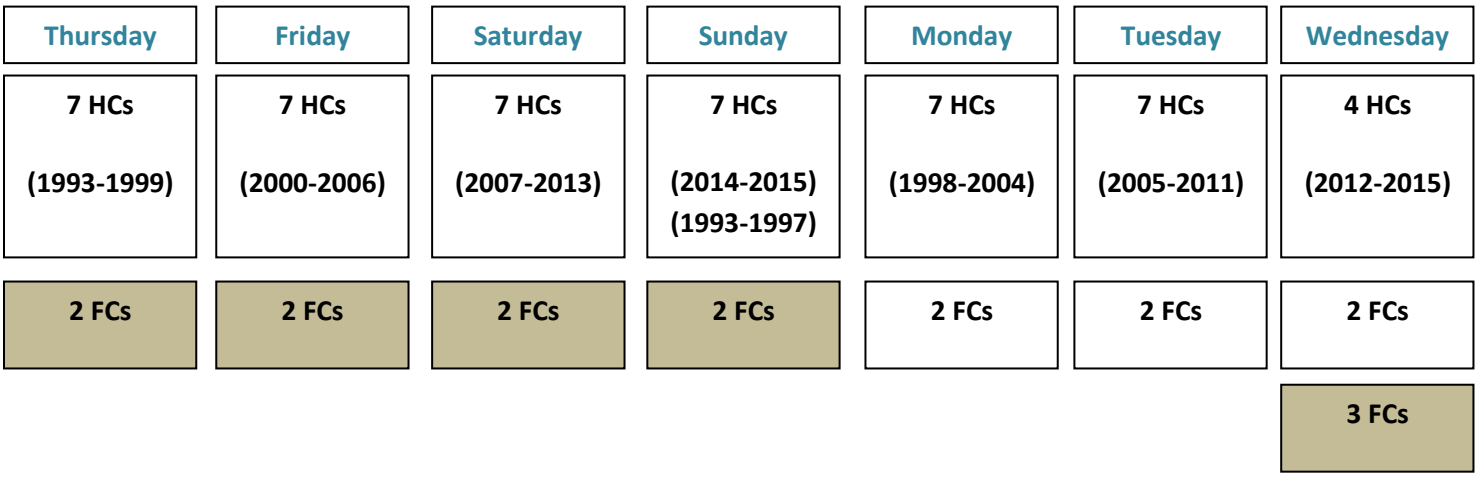

Figure 3: Weekly load balancing to produce 6-member forecast and 2-member hindcast. The shaded boxes are optional forecasts needed for daily forecasts and form a perfect load-balanced system.

5.5 Model Output and Post-processing

Output fields from different components of the coupled model go through different output processing streams. Of this land and atmospheric fields go through a highly user-configurable STASH processing system. The land and atmospheric fields are written to a same set of files which are re-initialized every 18 days to limit the file size. The ocean-seaice output is handled separately even though the NEMO-CICE is compiled into a single executable. The NEMO uses a XML file to define the file names, different output grids (viz. T-grid, U-grid, V-grid), levels on which output is desired etc. The XML file is parsed using set of codes distributed with NEMO source code. CICE model uses a FORTRAN namelist file to define the list of output variables and the frequency of output. The complete list of output files, list of variables in each file and frequency of output is given in Appendix B. The UM files are simply moved from the work

directory to the backup directory. Post processing of ocean files is a memory and time intensive job as discussed in Section 5.3. Current implementation of NEMO 3.4 does not use an IO server to gather output from individual processors; this will be updated in next configuration upgrade, where XIOS server will be used to combine the model output during runtime.

5.6 Extended Range Forecast Strategy and Products

Beginning monsoon season of 2018, NCMRWF has started producing and sharing the extended range forecast up to four weeks to Indian Meteorological Department (IMD) and National Centre for Polar and Ocean Research (NCPOR). Each week forecasts are generated by running the coupled model for 36-days of simulation to facilitate preparation of weekly-mean anomalies up to 4-week of lead times. The definition of week is set with Friday as its start day to be consistent with the weekly forecast issued by IMD on every Thursday. For generating spread in the forecast members an ensemble strategy based on both lagged startdates (initial conditions differing by adjacent days) and physical perturbations is adopted. The stochastic kinetic energy backscatter scheme (SKEB) used to introduce physical perturbations is documented in (Bowler et al. 2009)For a week, every Monday, Tuesday and Wednesday, forecasts are initialized using land-atmosphere and ocean-seaice analysis prepared at NCMRWF. All model runs are completed by Thursday forenoon. With two perturbed members per startdate this produces a 6-member ensemble. Each week23 years (1993-2015) of hindcasts, also up to 36-days of simulation are also carried out to calculate climatology for the weekly forecasts. The startdates for the hindcasts are fixed at 1, 9, 17 and 25 calendar day of each month. The production cycle is designed to facilitate completion of both forecast and hindcast by Thursday of each week by spreading the hindcasts over 7-days as described in Section 5.4. For computation of anomalies, the hindcast startdate nearest to the middle of the forecast startdates is used. Since a lagged-forecast ensemble strategy is used, up to first 4-days of forecast need to be discarded to produce forecasts valid from week beginning Friday. 36-days of simulation allows computation of forecasts up to 4-week of lead time.

5.6.1 Atmospheric Parameters

A sample forecast for weekly averaged precipitation up to 4-weeks of lead-times for the week starting from 6th July, 2018 is shown in Figure 4. Anomalies are shown in Figure 5 and are computed by subtracting the model climatology from 23-years of hindcasts initialized from

nearest available startdates but valid for the same four weeks as in Figure 4.For instance, the forecasts in these plots are initialized on 2nd, 3rd, and 4th of July with hindcast initialized on 1st July of each year. Figure 4shows a high precipitation zone over eastern part of Monsoon Trough zone (active monsoon conditions), which is intensifying by week-2. By week-3 and week-4 the precipitation gradually weaken over most party of India and is confined to the Himalayan foothills (break monsoon conditions). The signal of precipitation is much clearer in anomalies-forecast shown in Figure 5. It shows active conditions over central India which intensifies in week-2 forecast. Third week forecast shows positive weak anomalies moving slight northward, which by week-4 has diminished. By then the Bay of Bengal and parts of central India shows negative anomaly (break conditions). This is a typical case of moving from active to break phase. Corresponding observed anomalies are shown in Figure 6. It can be seen that in this case the model is able to capture the change of phase 3-weeks in advance for this forecast when compared against observed anomalies. It is important to see that model is able to respond to both initial conditions and boundary conditions during the seasonal cycle of monsoon. By averaging over all hindcast years a climatological forecast for all startdates from May-September is prepared. Figure 7 shows 4-weeks of precipitation simulation from each such startdate against the observations climatology. It can be seen that while there is slight over-prediction during May and under-prediction during July-August, hindcasts initialized from different startdates capture reasonably well the seasonal cycle of monsoon. Further, hindcasts initialized from 1st May to 1st June shows the climatological onset is captured several weeks in advance. Although there seems to be reduced intraseasonal variability in model forecasts, model shows higher ISV during June-August compared to May and September. Here, stochastic kinetic energy backscatter (SKEB) scheme is used to physically perturb the members. A typical spread of precipitation seen during peak monsoon period is shown in Figure 8 and Figure 9. Figure 8 shows week-4 forecast valid for 3rd-9th August for 4 forecast members initialized from same startdate. Large spread is seen by week-4. While large scale spatial pattern of ensemble mean and individual member is similar, large differences are seen over head Bay of Bengal and Indo-Gangetic plains (Figure 9).

In winter ERP of surface temperature (maximum and minimum) are very useful for agricultural applications. A sample anomaly prediction of surface temperatures are shown here. Figure 10 and Figure 11 are the weekly mean daily maximum and minimum temperature forecast anomalies respectively for the period 4th-31st January 2019. The anomalies are computed from

model climatology using hindcasts initialized on 1st January of each hindcast year in this case. Forecast for this period shows up to 2 ^{0}C of negative (cooler) anomalies in daily maximum temperature over northwestern and central parts of India in week-1. Week-2 shows anomalous positive (warmer) maximum temperatures over most parts of India which peaks by week-3 over southern peninsular India. The minimum temperatures show large cooler anomalies over central and southern India, which are sustained with reduced strength particularly over central India even in week-4.

5.6.1 Oceanic Parameters

Figure 12 and Figure 13 shows multi-week forecast of weekly averaged sea surface temperature and its anomalies with respect to climatological forecast for week starting from 3rd May 2019. The pre-monsoon period clearly shows temperatures in central Bay of Bengal rising from ~29^{0}Cto more than 31 ^{0}C within a span of 3-4 weeks. However, gradual cooling is seen in forecasts from week-3 in South China Sea. Forecast anomalies shown in Figure 13 also indicate anomalous warm waters in the South China Sea and the western equatorial Indian Ocean in all weeks. Anomalies in the Bay of Bengal also show large variability in sea surface temperatures with of~1.5 ^{0}C cool anomalies in week-1 reversing in sign and showing up as ~1.5 ^{0}C of warm anomalies by week-4.

5.6.2 Seaice Parameters

The extended range prediction system implemented here provides useful information about the variability of seaice up to 4-weeks in advance for Polar Regions. The forecast charts and data are being shared with NCPOR. Figure 14 and Figure 15 shows a sample forecast of full fields and also the anomalies for seaice concentrations expressed as fraction of area-covered in Antarctic region for the period 2nd-29th November 2018. Large parts of seas in the Antarctic region can be seen to be covered with seaice during this period. The concentration is reducing by week-4. This can also be seen in Figure 15 which shows anomalously less seaice south of the Atlantic Ocean in all weeks. Together such information helps in providing estimate of currently evolving situation and put it in perspective with climatological conditions in the region. Similarly, Figure 16 and Figure 17 show seaice concentration and anomalies forecast in the Arctic region. Here, the seaice is seen to be increasing by week-4. However, negative seaice anomalies in week-4 suggest that the build of seaice is less compared to climatology, as indicated by model forecasts.

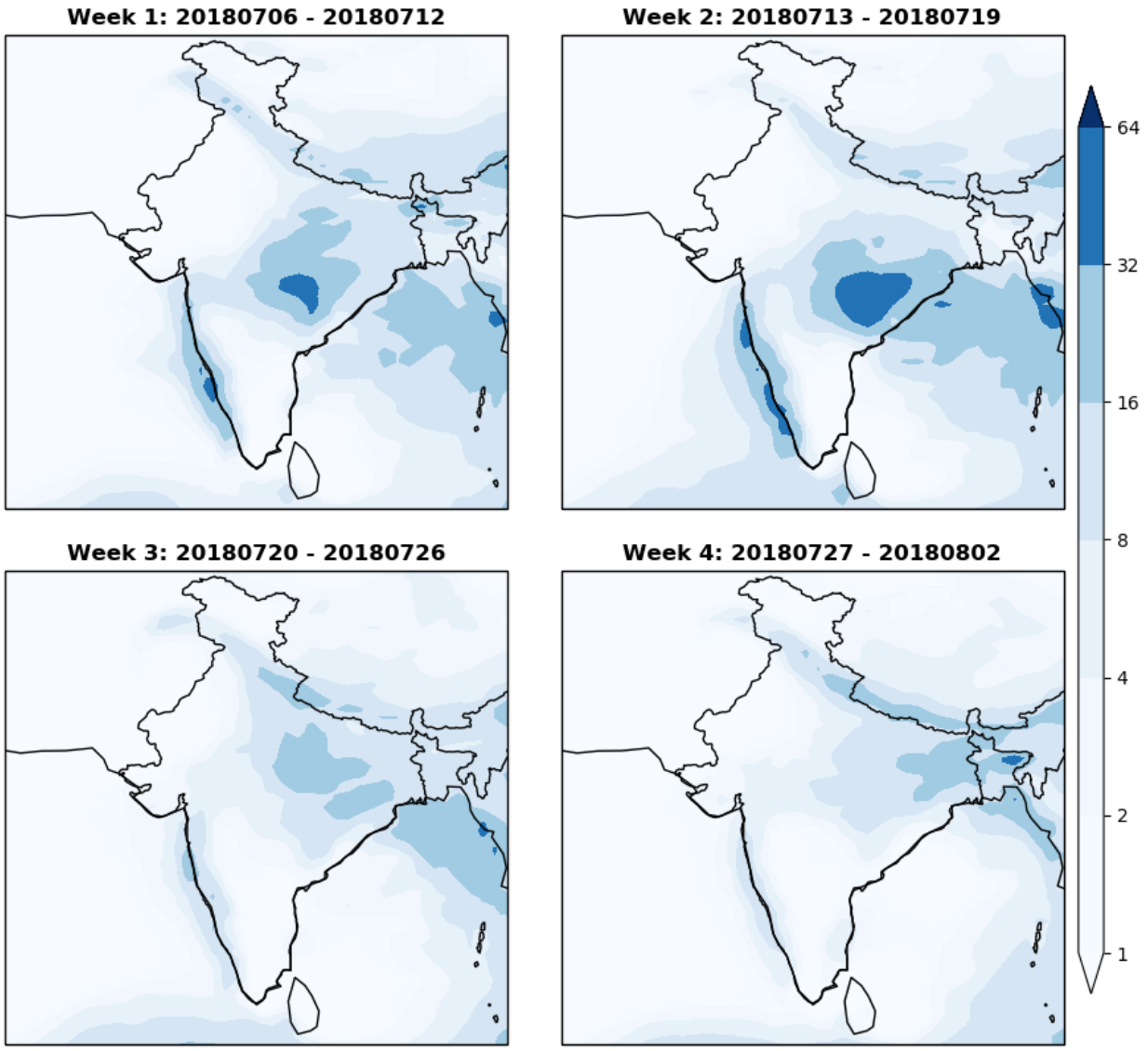

Figure 4: Weekly average precipitation (mm/day) from forecasts initialized on 2-4 July, 2018

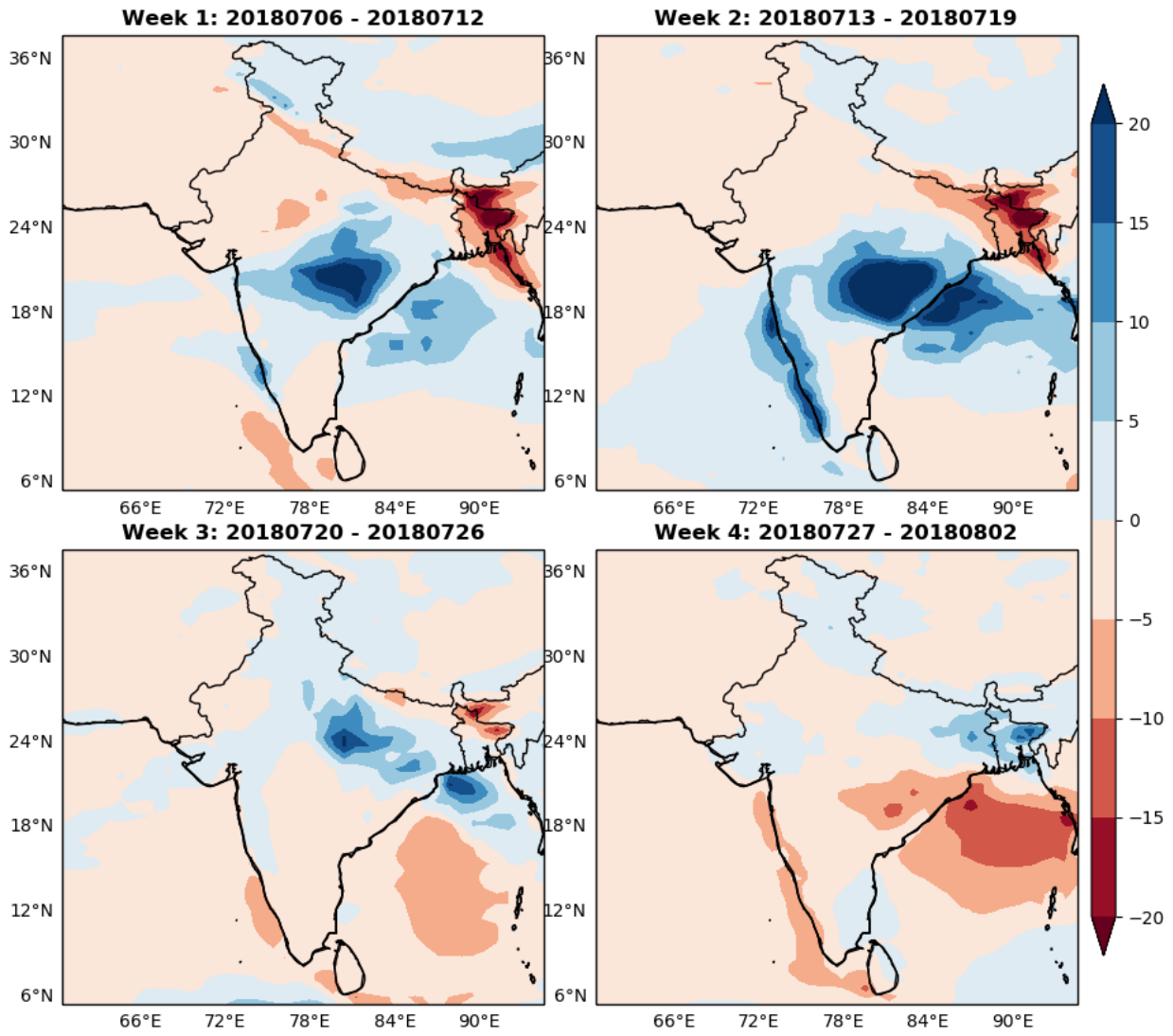

Figure 5: Weekly average precipitation anomalies (mm/day) from forecasts initialized on 2-4 July, 2018

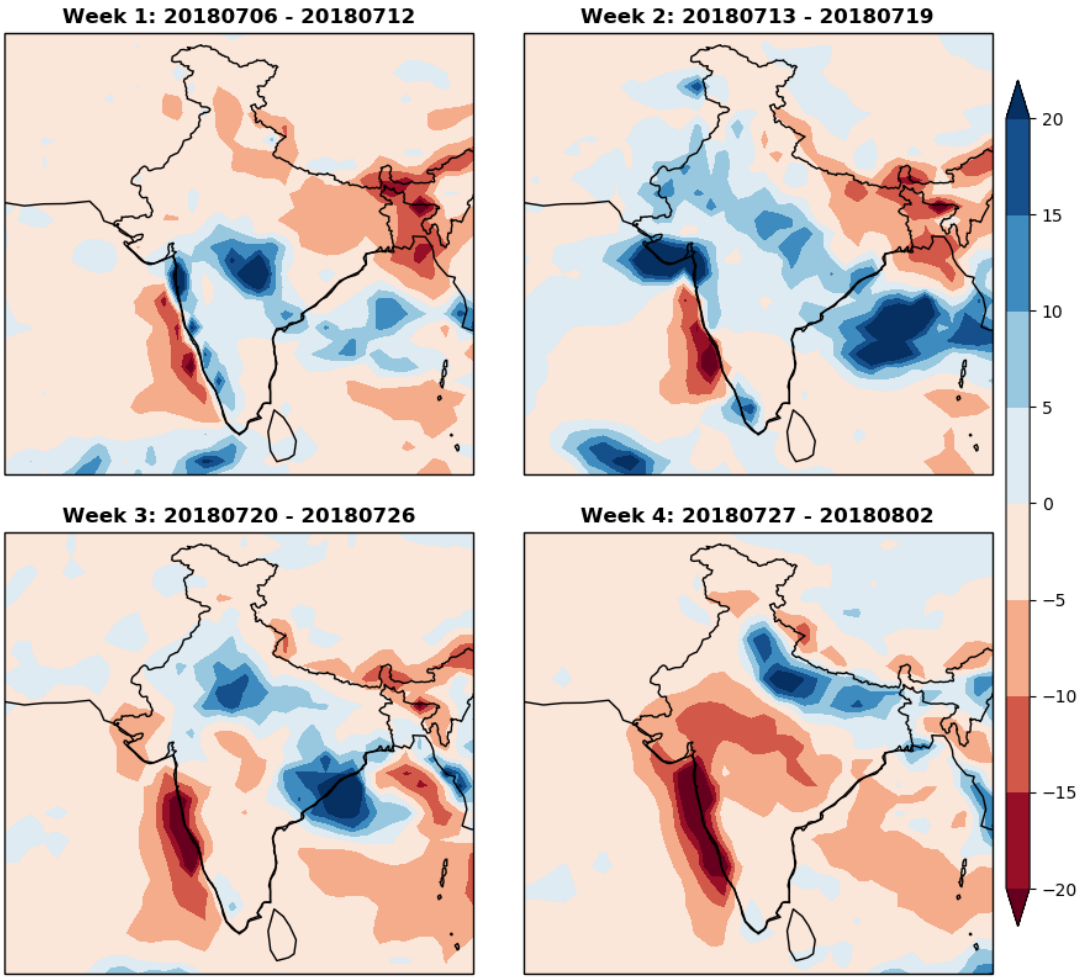

Figure 6: Same as Figure 5 but for observations from merged rainfall product

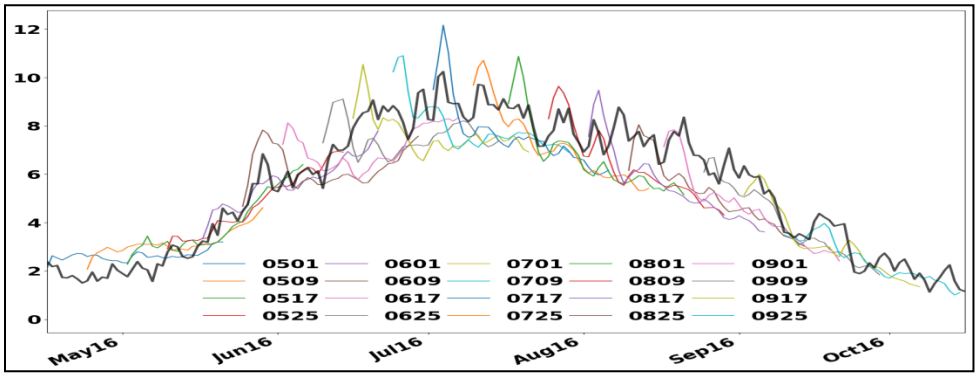

Figure 7: 4-week precipitation forecasts for all startdates averaged over all hindcast years. Solid black line shows observations.

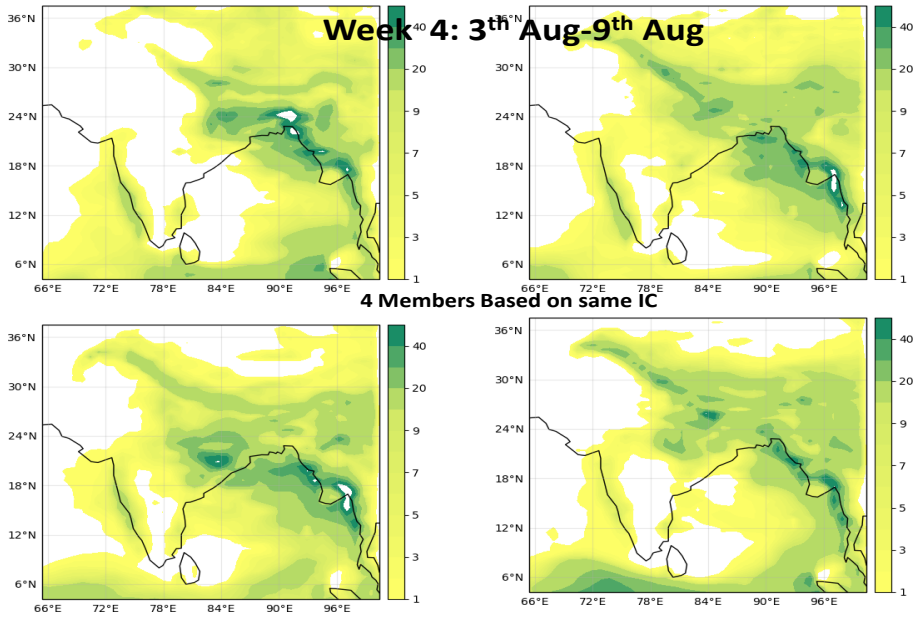

Figure 8: Week-4 forecast from 4 individual members for the week 3-9 August, 2018

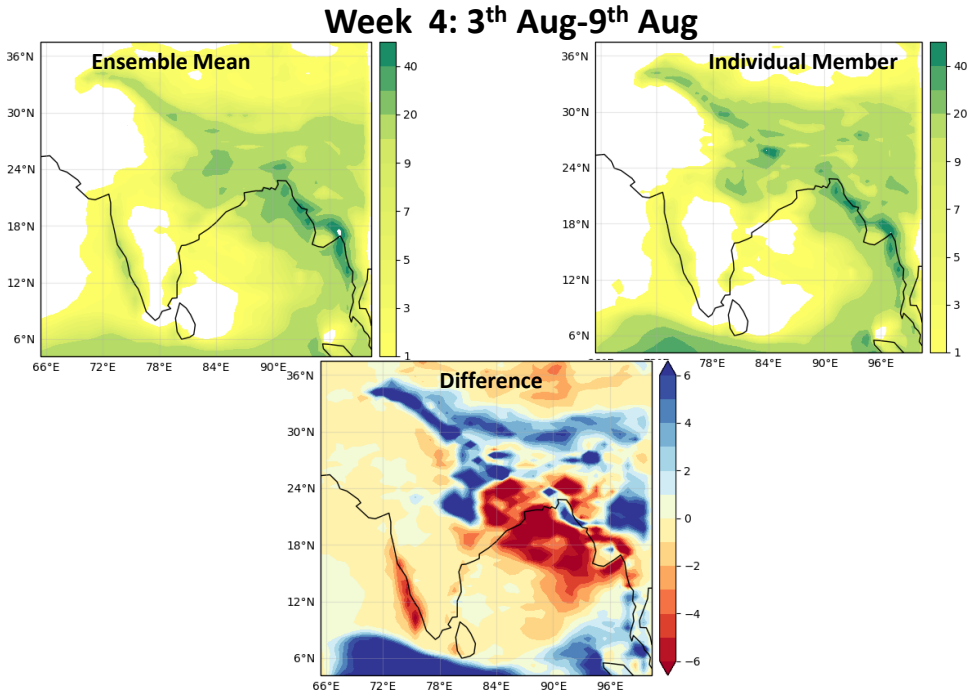

Figure 9: Week-4 forecast from ensemble mean, individual member. Difference of member from ensemble-mean is also shown.

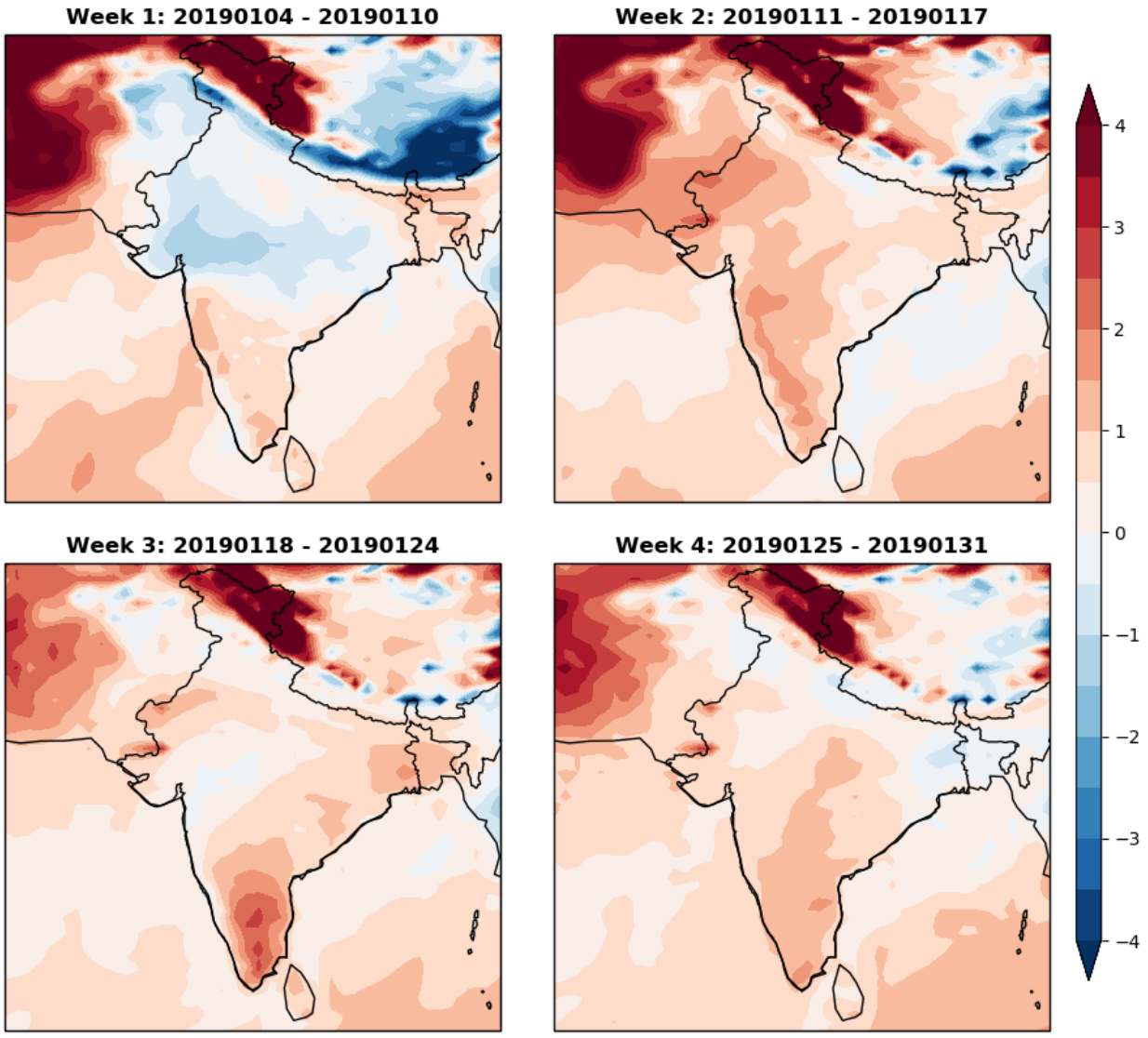

Figure 10: Weekly average daily maximum temperature anomalies (^{0}C) from forecasts initialized on 31 December 2018 to 2 January 2019.

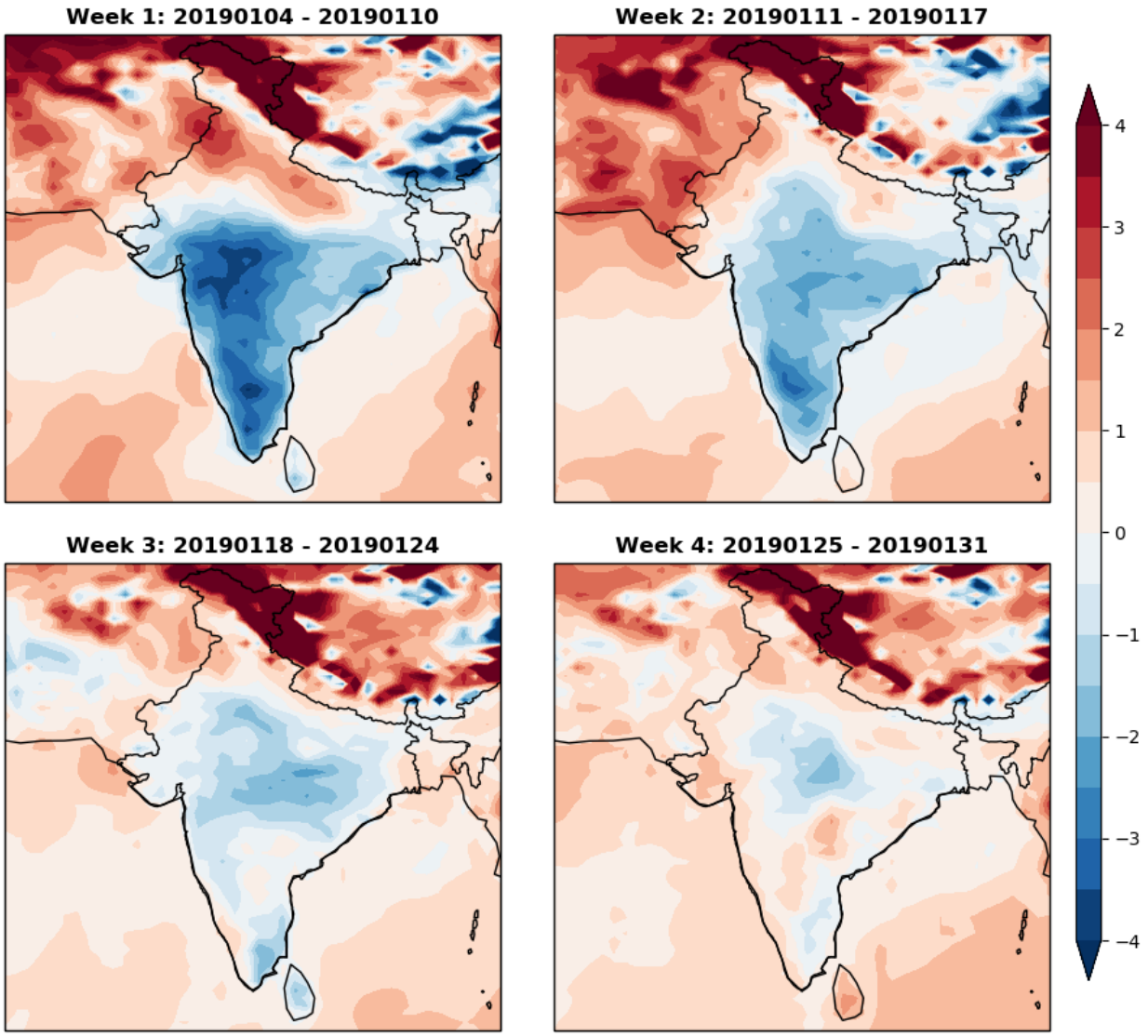

Figure 11: Weekly average daily minimum temperature anomalies (0C) from forecasts initialized on 31 December 2018 to 2 January 2019.

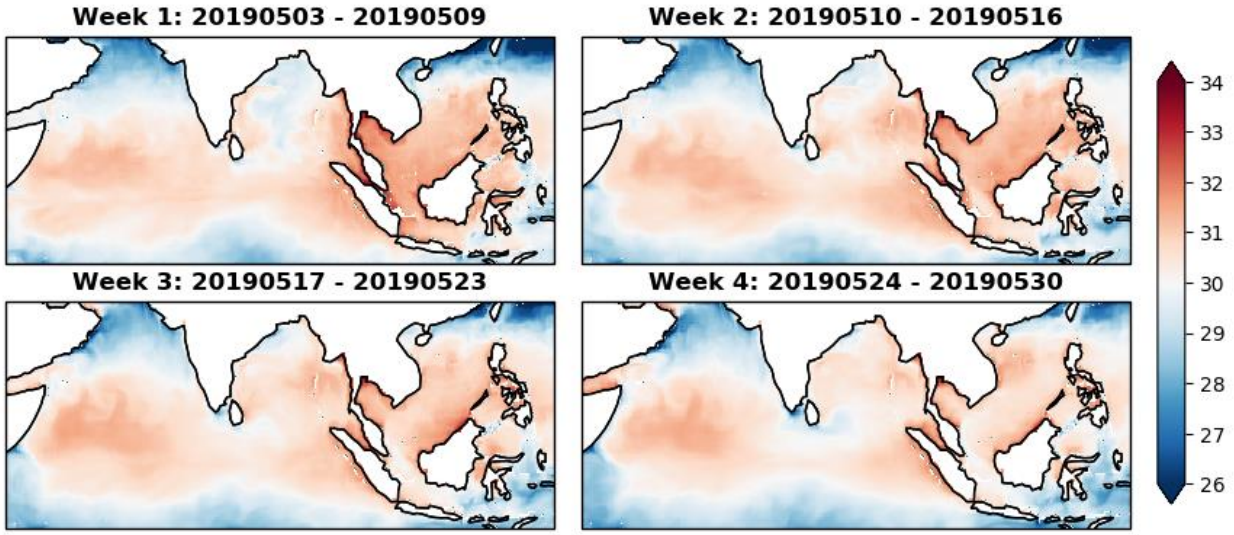

Figure 12: Weekly average forecast sea surface temperatures (^{0}C) from forecasts initialized on 29 April-1 May, 2019

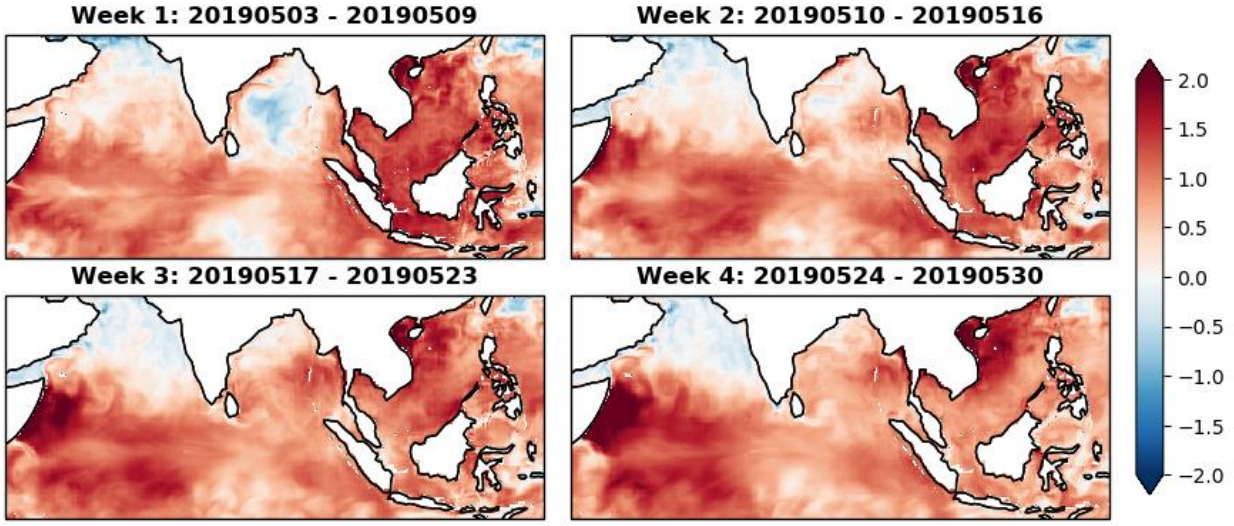

Figure 13: Weekly average forecast sea surface temperatures anomalies (^{0}C) from forecasts initialized on 29 April-1 May, 2019

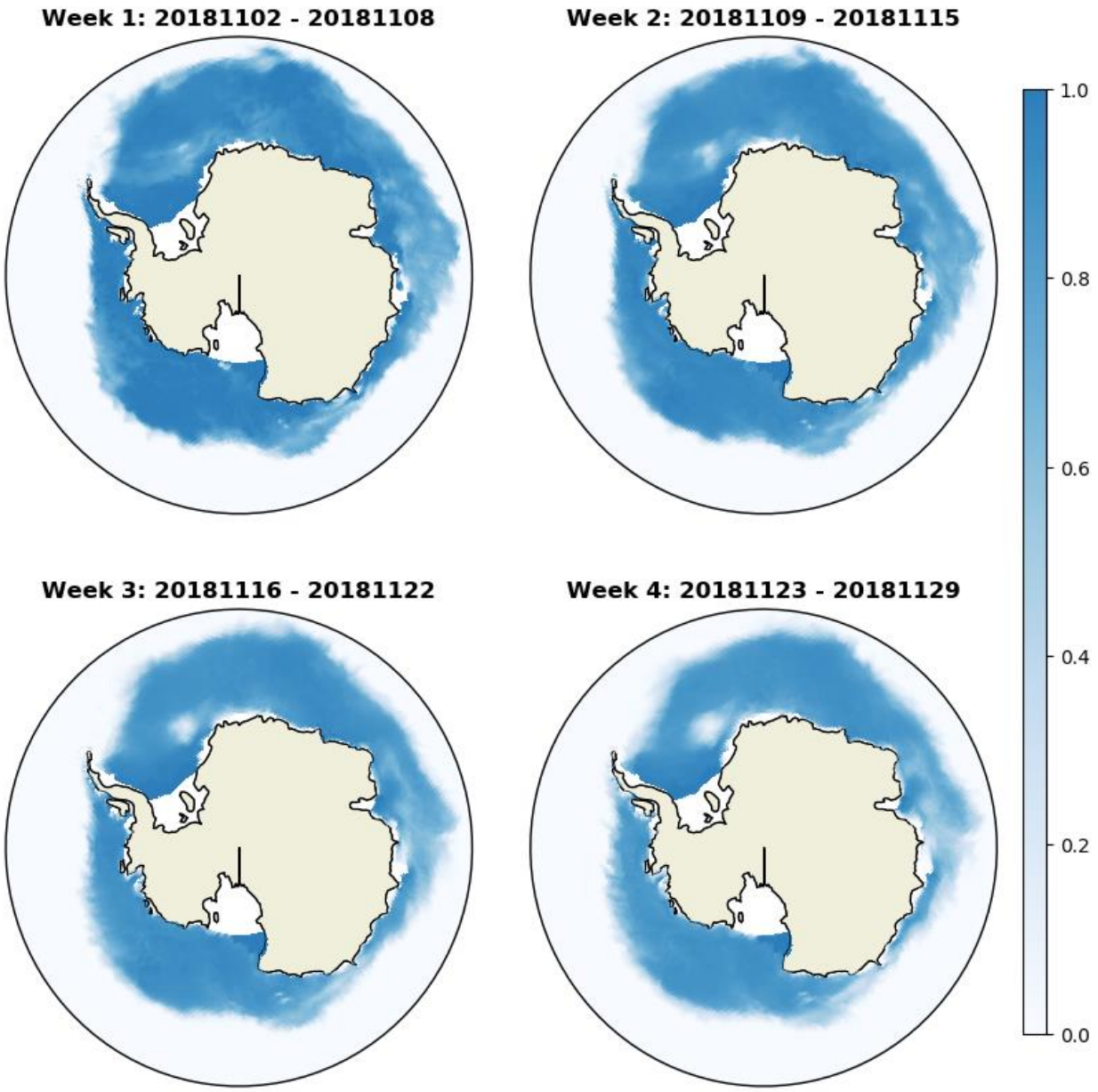

Figure 14: Weekly average forecast sea ice concentration (fraction) from forecasts initialized on 29 -31 October, 2018 in Antarctic region

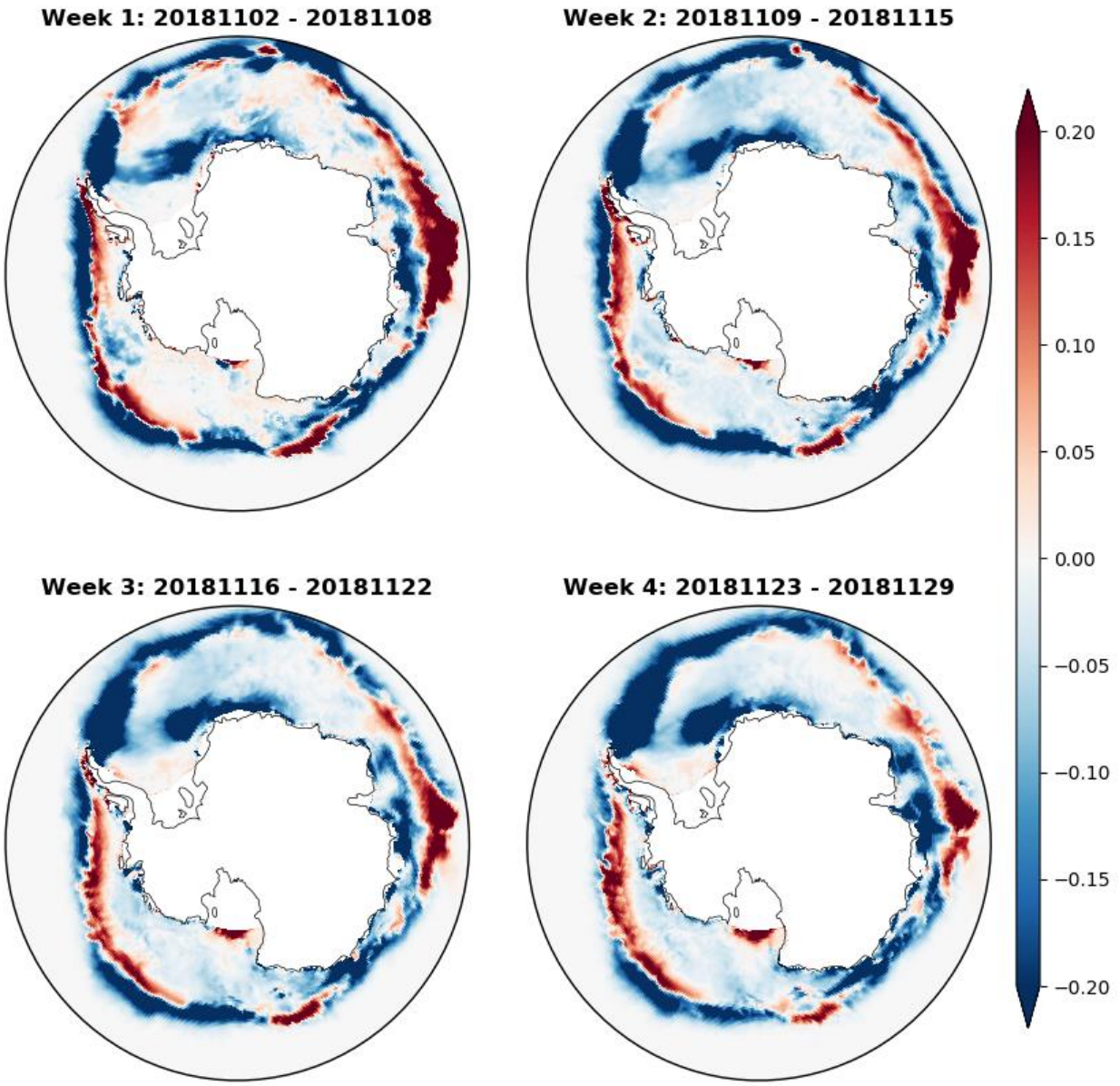

Figure 15: Weekly average forecast sea ice concentration (fraction) anomalies from forecasts initialized on 29 -31 October, 2018 in Antarctic region

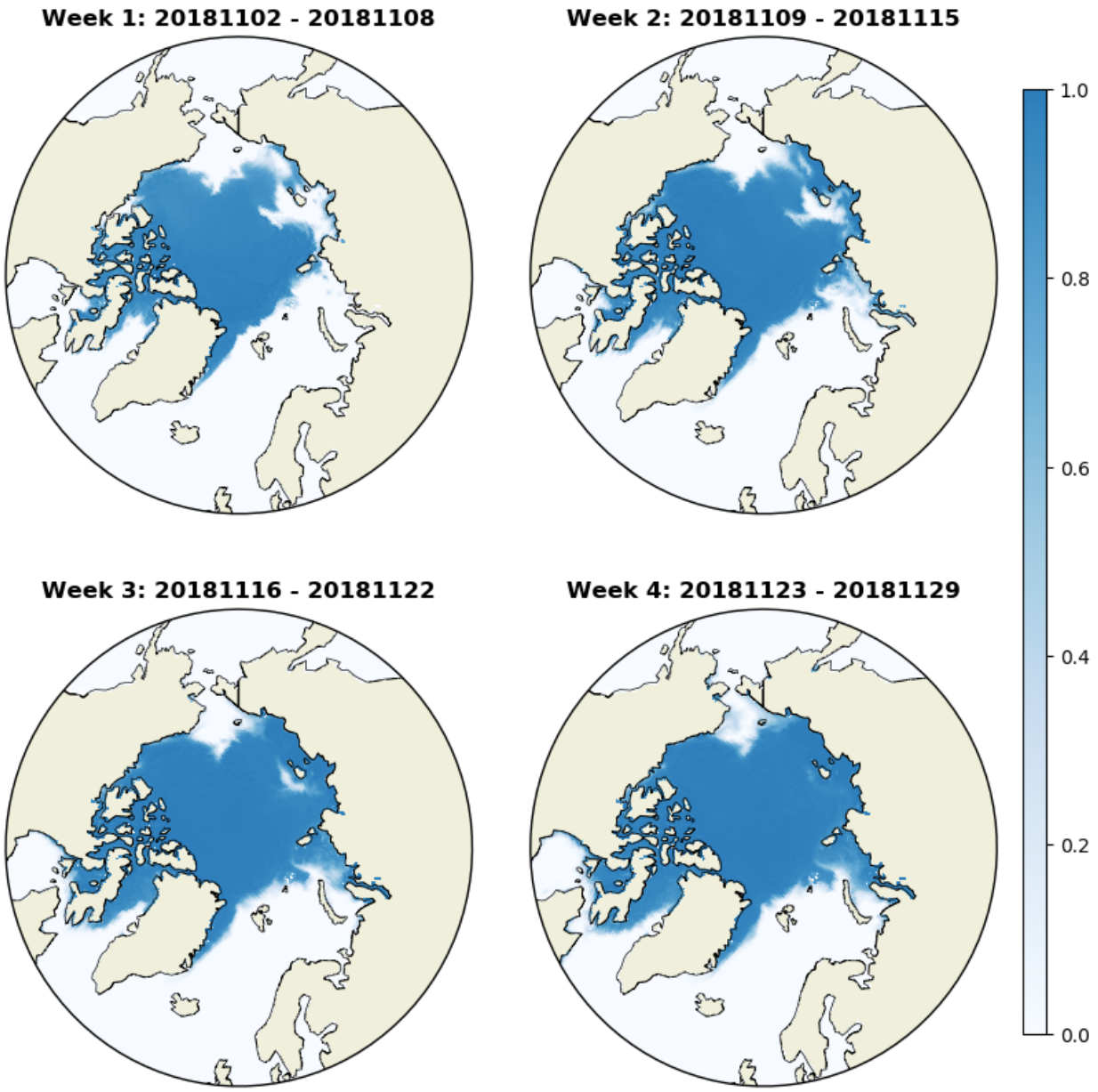

Figure 16: Weekly average forecast sea ice concentration (fraction) from forecasts initialized on 29 -31 October, 2018 in Arctic region

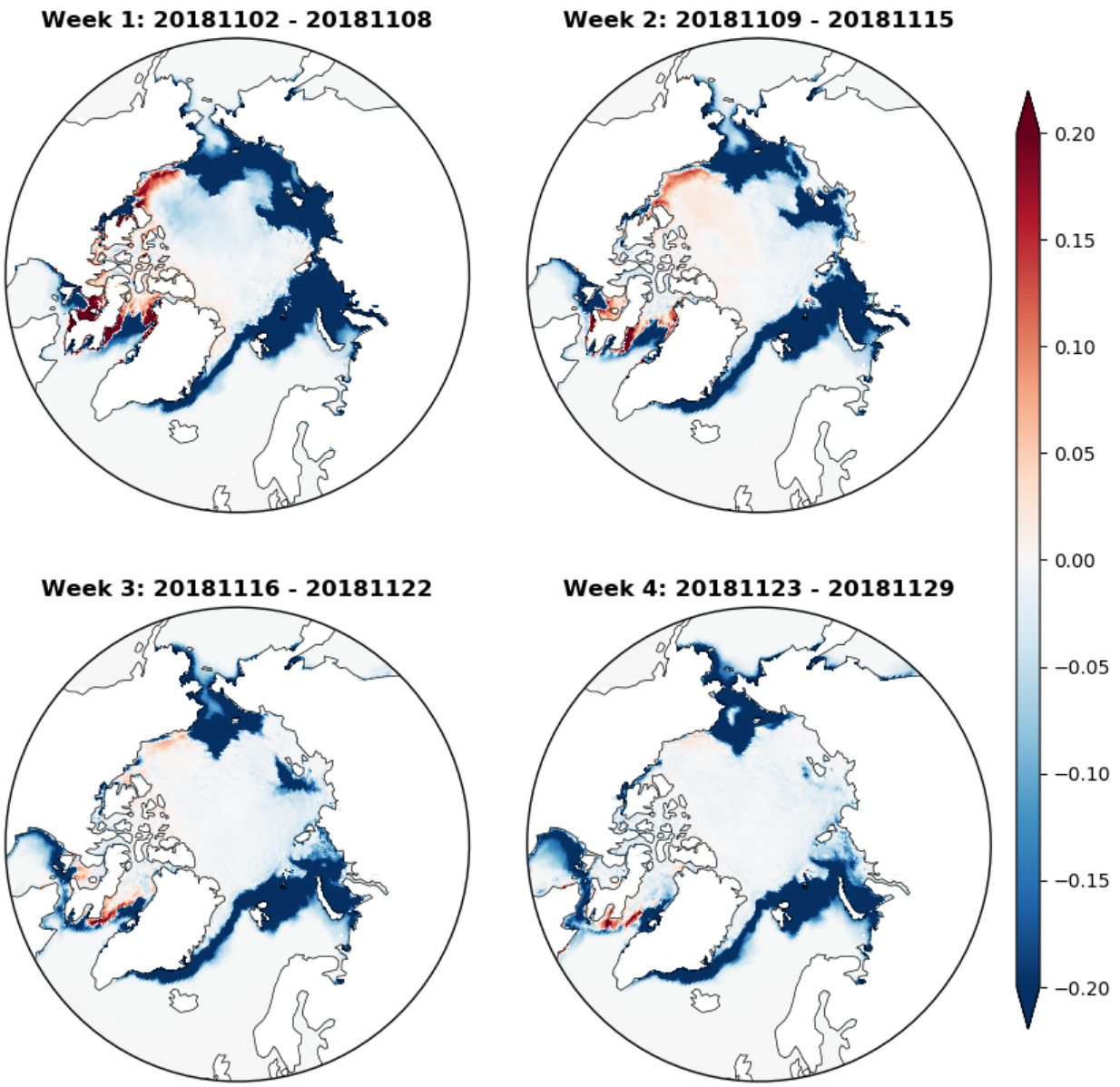

Figure 17: Weekly average forecast sea ice concentration (fraction) anomalies from forecasts initialized on 29 -31 October, 2018 in Arctic region

6 Seasonal Forecast Suite and hindcasts

The seasonal forecasts are generated by running the coupled configuration described above for seven months of simulation time. For demonstration purpose the seasonal suite was tested for monsoon seasonal rainfall anomaly forecasts for JJAS period starting April and May startdates. The sample April forecasts were based on twenty-five member ensemble based on 7th to 11thAprilstartdates each having five physically perturbed (SKEB) members. A six-member per

startdate hindcasts are also produced initialized on 9th April for the period 1993-2015. Here we analyze the skill of the model in capturing the Indian summer monsoon rainfall (ISMR) based on April initial conditions. Figure 18a shows the JJAS mean rainfall over Indian mainland both from the seasonal forecast system and observations from merged rainfall product. The model shows a marginal dry bias which is consistent in all years. However, it can be seen that inter-annual variability of the rainfall is captured well by the seasonal forecasts at 2-month of lead-time. Figure **18**b shows the anomalies of hindcasts with respect to the model climatology and equivalent observed anomalies. It can be seen that 10 out of 18 years the model is able to capture the sign of significant anomalies correctly. Experimental JJAS 2019 monsoon forecasts from April/May were produced and shared with IMD (plots not shown here) in realtime.

a)

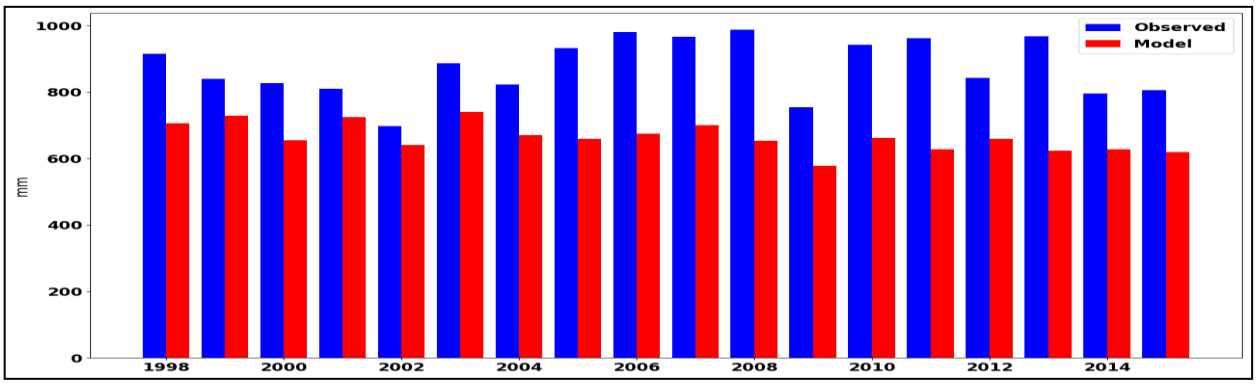

b)

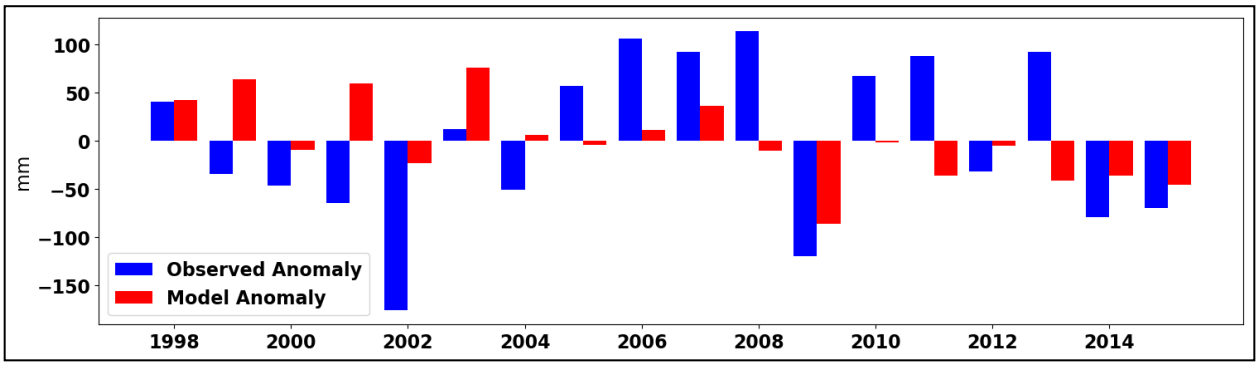

Figure 18: Average precipitation (mm) over Indian mainland accumulated for June-September (a) and anomalies with respect to 23 year climatology (b) for forecasts based on April initial conditions and observations.

7 Summary

Coupled model based Sub-seasonal to Seasonal range forecast suites have been implemented on Mihir HPC at NCMRWF. These forecast systems form key part of the seamless modeling strategy adopted by NCMRWF for forecast across time and spatial scales from days-to-season. The forecast suites are based on a coupled model in which each of the land, atmosphere, ocean and seaice components of the earth system is represented by a separate model. The individual models are coupled using OASIS coupler which uses remapping weights generated using relevant SCRIP algorithms for interpolation of fields at the coupling interface. The coupling frequency is set to 3-hourly. A key component of a sub-seasonal to seasonal forecast system is a set of hindcasts which is used to assess the skill of the system and is needed for computing anomalies and to carry out any further calibration of the forecasts. Accordingly, a hindcast set of 23 years for the period 1993-2015 is generated on Mihir HPC. The hindcasts are physically perturbed to generate a 6-member ensemble for each hindcast startdate. The forecast ensemble is generated using both physical perturbations and using forecast from lagged startdates. The land, atmosphere, ocean and seaice forecasts are initialized from respective NCMRWF operational analyses. The land-atmosphere in hindcasts is initialized from ECMWF ERA-Interim reanalysis, while GloSea ocean-seaice reanalysis is used for ocean-seaice component. The extended range prediction system is running in realtime since 2018 monsoon season, and weekly anomalies up to four weeks are produced every week. The seasonal forecast system is implemented in April 2019. For ERP system forecasts are initialized every Monday, Tuesday and Wednesday using the same model configuration and parameterizations as in the hindcasts. The workflows of ERP/Seasonal suite in both forecast and hindcast mode have been described in detail. Key differences in the forecast and hindcast workflows arises due to the difference in the source, preparation and reconfiguration of initial conditions; difference in scheduling of forecasts and hindcasts; and difference in the number and frequency of output variables. Lists of output variables from each of the component model have been compiled for both hindcasts and forecasts.

A subjective evaluation of all multi-week forecasts during monsoon period in 23-years hindcast set shows that the model captures the multi-week temporal variability of precipitation over Indian mainland reasonably well. Preliminary evaluation of seasonal hindcasts initialized

from April startdates shows that model is able to capture inter-annual variability by 2-month lead JJAS precipitation forecasts; accuracy of the model in capturing the sign of mean summer precipitation anomalies averaged over Indian mainland is over 50%. An objective and detailed analysis on the skill of the model is being carried out for both extended and seasonal scale. A large number of products are developed around the ERP suite including major components of the earth system. Sample multi-week forecasts of precipitation, daily minimum and maximum temperatures, SSTs, seaice in Arctic and Antarctic regions are included here. Weekly averaged forecast charts for up to 4-weeks of lead-times are shared with inter-ministerial institutions: IMD and NCPOR. Together with Global Forecast System (GFS/CFS) based ERP system operational at IITM/IMD, UM based ERP system described here provides valuable input to the several stakeholders dependent on the weather forecasts at scales beyond medium range. Further improvements such as increasing the resolution for the ERP system and increasing the number of ensemble members for the extended/seasonal forecasting system are under development.

Acknowledgments

The authors are thankful to Secretary, MoES for his constant encouragement for development and implementation of UM-based Extended/Seasonal scale Prediction System at NCMRWF. The authors like to acknowledge the Met Office and UM Partnership for providing access to UM and JULES model on Met Office Shared Repository Service (MOSRS). We also like to thank NEMO EU Consortium and CICE Consortium for providing respectively the ocean and sea-ice model codes. Acknowledgement is made for the use of ECMWF's ERA-Interim data for initializing the hindcasts. We are thankful to Joao Teixeira and Sean F. Milton from Met Office for their help and support in the implementation of the coupled model at NCMRWF.

References

Abhilash, S. et al. 2014. "Prediction and Monitoring of Monsoon Intraseasonal Oscillations over Indian Monsoon Region in an Ensemble Prediction System Using CFSv2." *Climate Dynamics*.

Ashok, Karumuri, Zhaoyong Guan, and Toshio Yamagata. 2001. "Impact of the Indian Ocean Dipole on the Relationship between the Indian Monsoon Rainfall and ENSO." *Geophysical Research Letters* 28(23): 4499–4502.

Bauer, Peter, Alan Thorpe, and Gilbert Brunet. 2015. "The Quiet Revolution of Numerical Weather Prediction." *Nature* 525(7567): 47.

Beckmann, A, and R Döscher. 1997. "A Method for Improved Representation of Dense Water Spreading over Topography in Geopotential-Coordinate Models." *Journal of Physical Oceanography* 27(4): 581–91.

Best, M J et al. 2011. "The Joint UK Land Environment Simulator (JULES), Model Description--Part 1: Energy and Water Fluxes." *Geoscientific Model Development* 4(3): 677–99.

Bitz, Cecilia M, and William H Lipscomb. 1999. "An Energy-Conserving Thermodynamic Model of Sea Ice." *Journal of Geophysical Research: Oceans* 104(C7): 15669–77.

Bowler, Neill E et al. 2009. "The Local ETKF and SKEB: Upgrades to the MOGREPS Short-Range Ensemble Prediction System." *Quarterly Journal of the Royal Meteorological Society* 135(640): 767–76.

Brunet, Gilbert et al. 2010. "Collaboration of the Weather and Climate Communities to Advance Subseasonal-to-Seasonal Prediction." *Bulletin of the American Meteorological Society* 91(10): 1397–1406.

Charney, Jg G, and J Shukla. 1981. "Predictability of Monsoons." In *Monsoon Dynamics*,.

Dee, Dick P et al. 2011. "The ERA-Interim Reanalysis: Configuration and Performance of the Data Assimilation System." *Quarterly Journal of the royal meteorological society* 137(656): 553–97.

Demott, Charlotte A, Nicholas P Klingaman, and Steven J Woolnough. 2015. "Reviews of Geophysics Atmosphere-Ocean Coupled Processes in the Madden-Julian Oscillation."

Edwards, J M, and A Slingo. 1996. "Studies with a Flexible New Radiation Code. I: Choosing a Configuration for a Large-Scale Model." *Quarterly Journal of the Royal Meteorological Society* 122(531): 689–719.

EPSTEIN, EDWARD S. 1969. "Stochastic Dynamic Prediction." *Tellus* 21(6): 739–59.

Gadgil, Sulochana, M Rajeevan, and Ravi Nanjundiah. 2005. "Monsoon Prediction: why yet Another Failure." *Curr. Sci* 88(9): 1389–1400.

Gadgil, Sulochana, and J Srinivasan. 1990. "Low Frequency Variation of Tropical Convergence Zones." *Meteorology and Atmospheric Physics* 44(1–4): 119–32.

Gaspar, Philippe, Yves Grégoris, and Jean-Michel Lefevre. 1990. "A Simple Eddy Kinetic Energy Model for Simulations of the Oceanic Vertical Mixing: Tests at Station Papa and Long-Term Upper Ocean Study Site." *Journal of Geophysical Research: Oceans* 95(C9): 16179–93.

Goswami, B N, and R S Ajaya Mohan. 2001. "Intraseasonal Oscillations and Interannual Variability of the Indian Summer Monsoon." *Journal of Climate* 14(6): 1180–98.

Gregory, D, and P R Rowntree. 1990. "A Mass Flux Convection Scheme with Representation of Cloud Ensemble Characteristics and Stability-Dependent Closure." *Monthly Weather Review* 118(7): 1483–1506.

Gupta, A, A K Mitra, and E N Rajagopal. 2019. "Implementation of Unified Model Based Global Coupled Modelling System at NCMRWF." *NMRF/TR/4/2014* 70.

Hewitt, H T et al. 2011. "Design and Implementation of the Infrastructure of HadGEM3: The next-Generation Met Office Climate Modelling System." *Geoscientific Model Development* 4(2): 223–53.

Hunke, E C, and J K Dukowicz. 1997. "An Elastic--Viscous--Plastic Model for Sea Ice Dynamics." *Journal of Physical Oceanography* 27(9): 1849–67.

Klingaman, N P, and S J Woolnough. 2014. "The Role of Air--Sea Coupling in the Simulation of the Madden--Julian Oscillation in the Hadley Centre Model." *Quarterly Journal of the Royal Meteorological Society* 140(684): 2272–86.

Klingaman, Nicholas P, Peter M Inness, Hilary Weller, and Julia M Slingo. 2008. "The Importance of High-Frequency Sea Surface Temperature Variability to the Intraseasonal Oscillation of Indian Monsoon Rainfall." *Journal of Climate* 21(23): 6119–40.

Kumar, Sumit et al. 2018. "Implementation of New High Resolution NCUM Analysis-Forecast System in Mihir HPCS."

Lee, Sun-Seon et al. 2015. "Predictability and Prediction Skill of the Boreal Summer Intraseasonal Oscillation in the Intraseasonal Variability Hindcast Experiment." *Climate Dynamics* 45(7–8): 2123–35.

Li, Xiaojing et al. 2016. "Assessment of Madden--Julian Oscillation Simulations with Various Configurations of CESM." *Climate Dynamics* 47(7–8): 2667–90.

Li, Yuanlong et al. 2018. "The Indian Summer Monsoon Intraseasonal Oscillations in CFSv2 Forecasts: Biases and Importance of Improving Air--Sea Interaction Processes." *Journal of Climate* 31(14): 5351–70.

Liu, Xiangwen et al. 2017. "MJO Prediction Using the Sub-Seasonal to Seasonal Forecast Model of Beijing Climate Center." *Climate Dynamics* 48(9–10): 3283–3307.

Lock, A P et al. 2000. "A New Boundary Layer Mixing Scheme. Part I: Scheme Description and Single-Column Model Tests." *Monthly weather review* 128(9): 3187–99.

Lorenz, Edward N. 1963. “Deterministic Nonperiodic Flow.” *Journal of the Atmospheric Sciences*.

Lott, François, and Martin J Miller. 1997. “A New Subgrid-Scale Orographic Drag Parametrization: Its Formulation and Testing.” *Quarterly Journal of the Royal Meteorological Society* 123(537): 101–27.

Maclachlan, C et al. 2015. “Global Seasonal Forecast System Version 5 (GloSea5): A High-Resolution Seasonal Forecast System.” *Quarterly Journal of the Royal Meteorological Society* 141(689): 1072–84.

McLaren, A J et al. 2006. “Evaluation of the Sea Ice Simulation in a New Coupled Atmosphere-Ocean Climate Model (HadGEM1).” *Journal of Geophysical Research: Oceans* 111(C12).

Megann, A et al. 2014. “GO5.0: The Joint NERC-Met Office NEMO Global Ocean Model for Use in Coupled and Forced Applications.” *Geoscientific Model Development* 7(3): 1069–92.

Mesinger, Fedor, and Akio Arakawa. 1976. “Numerical Methods Used in Atmospheric Models.”

Momin, Imranali M et al. “Impact of Altika Sea Level Anomaly Data on a Variational Assimilation System.” *Journal of Coastal Research*.

Rae, J G L et al. 2015. “Development of the Global Sea Ice 6.0 CICE Configuration for the Met Office Global Coupled Model.” *Geoscientific Model Development* 8(7): 2221–30.

Rajeevan, M, Sulochana Gadgil, and Jyoti Bhate. 2010. “Active and Break Spells of the Indian Summer Monsoon.” *Journal of earth system science* 119(3): 229–47.

Rajeevan, M, D S Pai, S K Dikshit, and R R Kelkar. 2004. “IMD’s New Operational Models for Long-Range Forecast of Southwest Monsoon Rainfall over India and Their Verification for 2003.” *Current Science*: 422–31.

Rajeevan, M, D S Pai, R Anil Kumar, and B Lal. 2007. “New Statistical Models for Long-Range Forecasting of Southwest Monsoon Rainfall over India.” *Climate Dynamics* 28(7–8): 813–28.

Rajeevan, M, C K Unnikrishnan, and B Preethi. 2012. “Evaluation of the ENSEMBLES Multi-Model Seasonal Forecasts of Indian Summer Monsoon Variability.” *Climate Dynamics* 38(11–12): 2257–74.

Robertson, Andrew W, Arun Kumar, Malaquias Peña, and Frederic Vitart. 2015. “Improving and Promoting Subseasonal to Seasonal Prediction.” *Bulletin of the American Meteorological Society* 96(3): ES49--ES53.

Scaife, A A, N Butchart, C D Warner, and R Swinbank. 2002. “Impact of a Spectral Gravity Wave Parameterization on the Stratosphere in the Met Office Unified Model.” *Journal of the atmospheric sciences* 59(9): 1473–89.

Sharmila, S et al. 2013. “Role of Ocean--Atmosphere Interaction on Northward Propagation of Indian Summer Monsoon Intra-Seasonal Oscillations (MISO).” *Climate dynamics* 41(5–6): 1651–69.

Shukla, J, and Daniel A Paolino. 1983. "The Southern Oscillation and Long-Range Forecasting of the Summer Monsoon Rainfall over India." *Monthly Weather Review* 111(9): 1830–37.

Simmons, Harper L, Steven R Jayne, Louis C St Laurent, and Andrew J Weaver. 2004. "Tidally Driven Mixing in a Numerical Model of the Ocean General Circulation." *Ocean Modelling* 6(3–4): 245–63.

Walters, David et al. 2017. "The Met Office Unified Model Global Atmosphere 6.0/6.1 and JULES Global Land 6.0/6.1 Configurations." *Geoscientific Model Development* 10(4): 1487–1520.

Waters, Jennifer et al. 2015. "Implementing a Variational Data Assimilation System in an Operational 1/4 Degree Global Ocean Model." *Quarterly Journal of the Royal Meteorological Society* 141(687): 333–49.

White, Christopher J et al. 2017. "Potential Applications of Subseasonal-to-Seasonal (S2S) Predictions." *Meteorological applications* 24(3): 315–25.

Williams, K D et al. 2015. "The Met Office Global Coupled Model 2.0 (GC2) Configuration." *Geoscientific Model Development* 8(5): 1509–24.

Wilson, Damian R et al. 2008. "PC2: A Prognostic Cloud Fraction and Condensation Scheme. I: Scheme Description." *Quarterly Journal of the Royal Meteorological Society: A journal of the atmospheric sciences, applied meteorology and physical oceanography* 134(637): 2093–2107.

Wilson, Damian R, and Susan P Ballard. 1999. "A Microphysically Based Precipitation Scheme for the UK Meteorological Office Unified Model." *Quarterly Journal of the Royal Meteorological Society* 125(557): 1607–36.

Wood, Nigel et al. 2014. "An Inherently Mass-Conserving Semi-Implicit Semi-Lagrangian Discretization of the Deep-Atmosphere Global Non-Hydrostatic Equations." *Quarterly Journal of the Royal Meteorological Society*.

Appendix A: List of initialized fields

Appendix A.1 Sources of initialized fields in forecast

Here the source of each initialized field is provided. The fields are categorized based on the source types. The fields initialized from input dump are listed below.

Table A.1: Fields read from input dump in forecast model

Sl. No.	Stash Code	Field Name
1	00002	U Compnt Of Wind After Timestep
2	00003	V Compnt Of Wind After Timestep
3	00004	Theta After Timestep
4	00010	Specific Humidity After Timestep
5	00012	Qcf After Timestep
6	00014	Conv Cloud Base Level No. After Ts
7	00015	Conv Cloud Top Level No. After Ts
8	00016	Conv Cloud Liquid Water Path
9	00020	Deep Soil Temp After Timestep
10	00021	Ccrad : Lowest Conv. Cld Base Layer
11	00022	Canopy Water After Timestep Kg/M2
12	00023	Snow Amount Over Land Aft Tstp Kg/M2
13	00025	Boundary Layer Depth After Timestep
14	00026	Roughness Length After Timestep
15	00028	Surface Zonal Current After Timestep
16	00029	Surface Merid Current After Timestep
17	00150	W Compnt Of Wind After Timestep
18	00211	Cca With Anvil After Timestep
19	00212	Ccrad : Ccw Passed To Radiation
20	00213	Canopy Conductance After Timestep
21	00214	Unfrozen Soil Moisture Frac After Ts
22	00215	Frozen Soil Moisture Frac After Ts
23	00225	Accumulated Leaf Turnover Rate Pfts
24	00238	Surface Downward Lw Radiation W/M2
25	00239	Toa - Surf Upward Lw Radiation W/M2
26	00253	Density*R*R After Timestep
27	00254	Qcl After Timestep
28	00255	Exner Pressure (Rho) After Timestep
29	00259	Number Of Turbulent Mixing Levels
30	00260	Level Of Base Of Deep Stratocumulus
31	00261	Level Of Top Of Deep Stratocumulus
32	00262	Boundary Layer Convection Flag

33	00263	Sd Turbulent Fluc Layer1 Temp
34	00264	Sd Turbulent Fluc Layer1 Humidity
35	00265	Area Cloud Fraction In Each Layer
36	00266	Bulk Cloud Fraction In Each Layer
37	00267	Liquid Cloud Fraction In Each Layer
38	00268	Frozen Cloud Fraction In Each Layer
39	00269	Surface Zonal Current After Ts Pgrid
40	00270	Surface Merid Current After Ts Pgrid
41	00272	Rain After Timestep
42	00276	Exp Decay In Soil Sat Hyd Conducty
43	00278	Mean Water Table Depth M
44	00279	Surface Saturation Fraction
45	00280	Surface Wetland Fraction
46	00281	Saturation Frac In Deep Layer
47	00493	Convective Downdraught At Cld Base

The surface temperature field is processed into that over land, open sea and sea-ice and reconfigured into the astart file.

Table A.2: Fields processed from surface temperature

Sl No.	Stash Code	Field Name
1	00024	Surface Temperature After Timestep
2	00506	Land Surface Temp After Timestep
3	00507	Open Sea Surface Temp After Timestep
4	00508	Sea-Ice Surface Temp After Timestep

Each ancillary file used for initializing the model is listed below, along with all the associated fields and short description. Files which are used for updating the fields are highlighted as blue text and its update frequency is mentioned.

Table A.3: **Fields read from ancillary files**

Sl. No.	Stash Code	Field Name
$ANCILDIR_N216/orca025/iceberg_calving/gc1p0_anbag/v2/qrclim.icecalve		
1	00190	Iceberg Calving Field: Cpl Kg/M2/S
$ANCILDIR_N216/orca025/smc_snow/erai_plus_shifted_clim/periodic/v0/qrclim.smow		
2	00009	Soil Moisture Content In A Layer
$ANCILDIR_N216/orca025/land_sea_mask/etop01/v1/qrparm.landfrac		
3	00505	Land Fraction In Grid Box
$ANCILDIR_N216/orca025/land_sea_mask/etop01/v1/qrparm.mask		
4	00030	Land Mask (No Halo) (Land=True)

$ANCILDIR_N216/orca025/general_land/GlobAlbedo/v2/qrclim.land		
Updated every 5 day		
5	00243	Obs/Clim Snow-Free Surf Sw Albedo
$ANCILDIR_N216/orca025/orography/globe30/v5/qrparm.orog		
6	00005	Orographic Gradient X Component
7	00006	Orographic Gradient Y Component
8	00017	Silhouette Orographic Roughness
9	00018	Half Of (Peak To Trough Ht Of Orog)
10	00033	Orography (/Strat Lower Bc)
11	00034	Standard Deviation Of Orography
12	00035	Orographic Gradient Xx Component
13	00036	Orographic Gradient Xy Component
14	00037	Orographic Gradient Yy Component
$ANCILDIR_N216/orca025/soil_parameters/hwsd_vg/v3/qrparm.soil		
15	00040	Vol Smc At Wilting After Timestep
16	00041	Vol Smc At Crit Pt After Timestep
17	00043	Vol Smc At Saturation After Timestep
18	00044	Sat Soil Conductivity After Timestep
19	00046	Thermal Capacity After Timestep
20	00047	Thermal Conductivity After Timestep
21	00048	Saturated Soil Water Suction
22	00207	Clapp-Hornberger "B" Coefficient
23	00220	Snow-Free Albedo Of Soil
24	00223	Soil Carbon Content Kg C / M2
$ANCILDIR_N216/orca025/vegetation/fractions_igbp/v3/qrparm.veg.frac		
25	00216	Fractions Of Surface Types
$ANCILDIR_N216/orca025/vegetation/func_type_modis/v3/qrparm.veg.func		
Updated every 5 day		
26	00217	Leaf Area Index Of Plant Func Types
27	00218	Canopy Height Of Plant Func Types M
$ANCILDIR_N216/orca025/rivers_trip/sequence/etopo5/v2/qrparm.rivseq		
28	00151	River Sequence
29	00152	River Direction
$ANCILDIR_N216/orca025/rivers_trip/storage/fekete/v2/qrclim.rivstor		
30	00153	River Water Storage M2
$ANCILDIR_N216/orca025/hydrol_lsh/hydro1k/v1/qrparm.hydtopsd		
31	00275	Standard Devn In Topographic Index
$ANCILDIR_N216/orca025/hydrol_lsh/hydro1k/v1/qrparm.hydtopmn		
32	00274	Mean Topographic Index
$ANCILDIR_N216/aerosol_clims/biogenic/v4/qrclim.biog85		
Updated every 5 day		
33	00351	Clim Biogenic Aerosol Mmr
$ANCILDIR_N216/aerosol_clims/sslt/v4/qrclim.sslt85		
Updated every 5 day		
34	00357	Clim Sea Salt (Film Mode) Npm3

35	00358	Clim Sea Salt (Jet Mode) Npm3
$ANCILDIR_N216/aerosol_clims/biom/v4/qrclim.biom85		
Updated every 5 day		
36	00352	Clim Biomass-Burning (Fresh) Mmr
37	00353	Clim Biomass-Burning (Aged) Mmr
38	00354	Clim Biomass-Burning (In-Cloud) Mmr
$ANCILDIR_N216/aerosol_clims/sulp/v4/qrclim.sulp85		
Updated every 5 day		
39	00359	Clim Sulphate (Accumulation Mode)Mmr
40	00360	Clim Sulphate (Aitken Mode) Mmr
41	00361	Clim Sulphate (Dissolved) Mmr
$ANCILDIR_N216/aerosol_clims/ocff/v4/qrclim.ocff85		
Updated every 5 day		
42	00368	Clim Org C Fossil Fuel (Fresh) Mmr
43	00369	Clim Org C Fossil Fuel (Aged) Mmr
44	00370	Clim Org C Fossil Fuel (In-Cloud)Mmr
$ANCILDIR_N216/aerosol_clims/dust/v4/qrclim.dust85		
Updated every 5 day		
45	00362	Clim Dust Size Division 1 Mmr
46	00363	Clim Dust Size Division 2 Mmr
47	00364	Clim Dust Size Division 3 Mmr
48	00365	Clim Dust Size Division 4 Mmr
49	00366	Clim Dust Size Division 5 Mmr
50	00367	Clim Dust Size Division 6 Mmr
$ANCILDIR_N216/aerosol_clims/blck/v4/qrclim.blck85		
Updated every 5 day		
51	00355	Clim Black Carbon (Fresh) Mmr
52	00356	Clim Black Carbon (Aged) Mmr
$ANCILDIR_N216/ozone/sparc/1994-2005/v2/qrclim.ozone_L85_O85		
Updated every 30 day		
53	00060	Ozone **

Table A.4: Fields set to 0

Sl No.	Stash Code	Field Name
1	00031	Frac Of Sea Ice In Sea After Tstep
2	00032	Sea Ice Depth (Mean Over Ice) M
3	00095	Snow Amount Ovr Seaice Aft Ts Kg/M2
4	00155	Accumulated Surface Runoff Kg/M2
5	00156	Accumulated Sub-Surface Runoff Kg/M2
6	00157	Gridbox Areas M2
7	00171	Net Dn Sw Rad Flux:Open Sea: Cpl
8	00172	Net Dwn Sfc Sw Flux Blw 690Nm: Cpl
9	00173	Net Down Surface Lw Rad Flux: Cpl

10	00174	Net Dn Lw Rad Flux:Open Sea: Cpl
11	00176	X-Comp Surf & Bl Wind Str: Cpl N/M2
12	00177	Y-Comp Surf & Bl Wind Strl Cpl N/M2
13	00178	Wind Mix En'Gy Fl To Sea: Cpl W/M2
14	00179	Sfc Sh Flx From Open Sea: Cpl W/M2
15	00180	Sublim. Surface (Gbm): Cpl Kg/M2/S
16	00181	Evap From Open Sea: Cpl Kg/M2/S
17	00184	Heat Flx Through Sea Ice (W/M2): Cpl
18	00185	Heat Flx In Sea Ice Surface Mlt: Cpl
19	00186	Large Scale Rain Rate: Cpl Kg/M2/S
20	00187	Large Scale Snow Rate: Cpl Kg/M2/S
21	00188	Convective Rain Rate: Cpl Kg/M2/S
22	00189	Convective Snow Rate: Cpl Kg/M2/S
23	00191	10 Metre Wind Speed On C Grid: Cpl
24	00192	River Runoff: Cpl
25	00222	Net Energy Change This Period J/M**2
26	00235	Net Moisture Flux In Period Kg/M**2
27	00236	Tile Modified Infiltration Rate
28	00237	Downward Sw Radiation On Tiles W/M2
29	00242	Snow Beneath Canopy Kg/M2
30	00290	Daily Accumulated Lake Flux Kg/M2
31	00413	Sea Ice Concentration By Categories
32	00414	Sea Ice Thickness Gbm By Categories
33	00416	Sea Ice Snow Depth By Categories
34	00509	Sea Ice Albedo After Ts
35	00510	Mean Land Albedo After Ts
36	00511	Inland basin flow Atm Grid Kg/M2/S

Table A.5: Fields set to RMDI/IMDI

Sl No.	**Stash Code**	**Field Name**
1	00193	Pressure At Mean Sea Level: Cpl Pa
2	00390	Psiw Surface After Timestep
3	00397	Psiw Lid After Timestep
4	00490	Decoupled Screen Temp On Tiles K
5	00491	Decoupled Screen Temp On Sea/Ice K
6	00492	Time Since Transition S

Table A.6: Fields set to constant

Sl No.	**Stash Code**	**Field Name**
1	00230	Canopy Capacity On Tiles Kg/M2
2	00234	Roughness Length On Tiles M
3	00241	Canopy Snow Capacity Kg/M2

Table A.7: Fields initialised from other fields in input dump (field calculations)

Sl No.	Stash Code	Field Name
1	00049	Sea-Ice Temperature After Timestep
2	00229	Canopy Water On Tiles Kg/M2
3	00233	Surface Temperature On Tiles K
4	00240	Snow Amount On Tiles Kg/M2
5	00277	Integrated Gamma Distribution
6	00282	A_Fsat Hydrology Fitting Parameter
7	00283	C_Fsat Hydrology Fitting Parameter
8	00284	A_Fwet Hydrology Fitting Parameter
9	00285	C_Fwet Hydrology Fitting Parameter
10	00391	Vapour Mixing Ratio (Mv) After Ts
11	00392	Cld Liq Mixing Ratio (Mcl) After Ts
12	00393	Cld Ice Mixing Ratio (Mcf) After Ts
13	00394	Rain Mixing Ratio (Mr) After Ts
14	00395	Graupel Mixing Ratio (Mg) After Ts
15	00396	Ice Cry Mixing Rat. (Mcf2) After Ts
16	00415	Sea Ice Surf Temp By Categories (K)

Table A.8: Fields initialised from other fields in either the input dump or ones already processed into the output dump (field dependent calculations)

Sl No.	Stash Code	Field Name
1	00376	Snow Depth On Ground On Tiles (M)
2	00387	Etadot After Timestep
3	00388	Thetavd After Timestep
4	00389	Dry Rho After Timestep
5	00398	Exner Surf After Timestep

Appendix A.2 Fields initialized differently in hindcasts

The ECMWF ERA-Interim is used for initializing the hindcasts. Only twelve fields are read from startdumps in hindcasts as listed in Table 1: Variables from ECMWF reanalysis used for initializing the **hindcasts**. However both hindcasts and forecasts uses the same model and thus require same set of initialized variables. Thus the fields not present in ECMWF startdumps are initialized to some constants or computed from other fields in input dump.

Table A.9: Fields set to 0 only in hindcasts

Sl. No.	Stash Code	Field Name
1	00014	Conv Cloud Base Level No. After Ts
2	00015	Conv Cloud Top Level No. After Ts
3	00016	Conv Cloud Liquid Water Path
4	00021	Ccrad : Lowest Conv. Cld Base Layer
5	00022	Canopy Water After Timestep Kg/M2
6	00028	Surface Zonal Current After Timestep
7	00029	Surface Merid Current After Timestep
8	00150	W Compnt Of Wind After Timestep
9	00211	Cca With Anvil After Timestep
10	00212	Ccrad : Ccw Passed To Radiation
11	00213	Canopy Conductance After Timestep
12	00214	Unfrozen Soil Moisture Frac After Ts
13	00215	Frozen Soil Moisture Frac After Ts
14	00229	Canopy Water On Tiles Kg/M2
15	00238	Surface Downward Lw Radiation W/M2
16	00239	Toa - Surf Upward Lw Radiation W/M2
17	00253	Density*R*R After Timestep
18	00255	Exner Pressure (Rho) After Timestep
19	00259	Number Of Turbulent Mixing Levels
20	00260	Level Of Base Of Deep Stratocumulus
21	00261	Level Of Top Of Deep Stratocumulus
22	00262	Boundary Layer Convection Flag
23	00263	Sd Turbulent Fluc Layer1 Temp
24	00264	Sd Turbulent Fluc Layer1 Humidity
25	00265	Area Cloud Fraction In Each Layer
26	00269	Surface Zonal Current After Ts Pgrid
27	00270	Surface Merid Current After Ts Pgrid
28	00272	Rain After Timestep
29	00493	Convective Downdraught At Cld Base

Table A. 10: Fields set to constant only in hindcasts

Sl No.	Stash Code	Field Name
1	00025	Boundary Layer Depth After Timestep
2	00026	Roughness Length After Timestep
3	00225	Accumulated Leaf Turnover Rate Pfts
4	00276	Exp Decay In Soil Sat Hyd Conducty

Table A.11: Fields initialised from other fields in input dump (field calculations) only in hindcasts

Sl No.	Stash Code	Field Name
1	00266	Bulk Cloud Fraction In Each Layer
2	00267	Liquid Cloud Fraction In Each Layer
3	00268	Frozen Cloud Fraction In Each Layer
4	00278	Mean Water Table Depth m
5	00279	Surface Saturation Fraction
6	00280	Surface Wetland Fraction
7	00281	Saturation Frac In Deep Layer

Appendix B: Model output fields common to forecasts and hindcasts

Appendix B.1: List of output land-atmosphere variables

Fields in file cplfca.pa20190501

Sl. No.	Stash Code	Field Name	Frequency
1	30456	Filtered Vorticity 850	6
2	30458	Filtered Vorticity Tc	6
3	16222	Pressure At Mean Sea Level	6
4	30201	U Compnt Of Wind On P Lev/Uv Grid	6
5	30202	V Compnt Of Wind On P Lev/Uv Grid	6
6	30455	Vorticity 850	6
7	30457	Vorticity Tc	6

Fields in file cplfca.pc20190501

Sl. No.	Stash Code	Field Name	Frequency
1	3209	10 Metre Wind U-Comp	24
2	5205	Convective Rainfall Rate Kg/M2/S	24
3	5206	Convective Snowfall Rate Kg/M2/S	24
4	16202	Geopotential Height On P Lev/P Grid	24
5	30301	HeavysideFn On P Lev/Uv Grid	24
6	4203	Large Scale Rainfall Rate Kg/M2/S	24
7	4204	Large Scale Snowfall Rate Kg/M2/S	24
8	2201	Net Down Surface Lw Rad Flux	24
9	15229	Potential Vorticity On Pressure Levs	24
10	16222	Pressure At Mean Sea Level	24
11	8023	Snow Mass After Hydrology Kg/M2	24
12	30205	Specific Humidity On P Lev/Uv Grid	24
13	3234	Surface Latent Heat Flux W/M2	24
14	3290	Surface Sensible Heat Flux On Tiles	24
15	3236	Temperature At 1.5M	24
16	30204	Temperature On P Lev/Uv Grid	24
17	3332	Toa Outgoing Lw Rad After B.Layer	24
18	9217	Total Cloud Amount Max/Random Overlp	24
19	1235	Total Downward Surface Sw Flux	24
20	5226	Total Precipitation Amount Kg/M2/Ts	24
21	30201	U Compnt Of Wind On P Lev/Uv Grid	24
22	30202	V Compnt Of Wind On P Lev/Uv Grid	24
23	3460	X-Comp Surface Bl Stress	24

Fields in file cplfca.pd20190501

Sl. No.	Stash Code	Field Name	Frequency
1	3209	10 Metre Wind U-Comp	24
2	3210	10 Metre Wind V-Comp	24
3	5205	Convective Rainfall Rate Kg/M2/S	24
4	5206	Convective Snowfall Rate Kg/M2/S	24
5	31	Frac Of Sea Ice In Sea After Tstep	24
6	16202	Geopotential Height On P Lev/P Grid	24
7	30301	HeavysideFn On P Lev/Uv Grid	24
8	4203	Large Scale Rainfall Rate Kg/M2/S	24
9	4204	Large Scale Snowfall Rate Kg/M2/S	24
10	16222	Pressure At Mean Sea Level	24
11	8023	Snow Mass After Hydrology Kg/M2	24
12	8223	Soil Moisture Content In A Layer	24
13	30205	Specific Humidity On P Lev/Uv Grid	24
14	24	Surface Temperature After Timestep	24
15	3236	Temperature At 1.5M	24
16	16203	Temperature On P Lev/P Grid	24
17	30204	Temperature On P Lev/Uv Grid	24
18	15215	Theta On Pv=+/-2 Surface	24
19	3332	Toa Outgoing Lw Rad After B.Layer	24
20	5226	Total Precipitation Amount Kg/M2/Ts	24
21	5216	Total Precipitation Rate Kg/M2/S	24
22	30201	U Compnt Of Wind On P Lev/Uv Grid	24
23	15201	U Wind On Pressure Levels B Grid	24
24	30202	V Compnt Of Wind On P Lev/Uv Grid	24
25	15202	V Wind On Pressure Levels B Grid	24

Fields in file cplfca.pe20190501

Sl. No.	Stash Code	Field Name	Frequency
1	16202	Geopotential Height On P Lev/P Grid	24
2	30201	U Compnt Of Wind On P Lev/Uv Grid	24
3	30202	V Compnt Of Wind On P Lev/Uv Grid	24

Fields in file cplfca.pf20190501

Sl. No.	Stash Code	Field Name	Frequency
1	3227	10 Metre Wind Speed On B Grid	24
2	3225	10 Metre Wind U-Comp B Grid	24
3	30428	Dry Mass Col Int U*Q Per Unit Area	24
4	30429	Dry Mass Col Int V*Q Per Unit Area	24

5	16202	Geopotential Height On P Lev/P Grid	24
6	30301	HeavysideFn On P Lev/Uv Grid	24
7	30205	Specific Humidity On P Lev/Uv Grid	24
8	30204	Temperature On P Lev/Uv Grid	24
9	3332	Toa Outgoing Lw Rad After B.Layer	24
10	30403	Total Column Dry Mass Rho Grid	24
11	30404	Total Column Wet Mass Rho Grid	24
12	30201	U Compnt Of Wind On P Lev/Uv Grid	24
13	30202	V Compnt Of Wind On P Lev/Uv Grid	24

Fields in file cplfca.pg20190501

Sl. No.	Stash Code	Field Name	Frequency
1	3209	10 Metre Wind U-Comp	24
2	3210	10 Metre Wind V-Comp	24
3	8258	Accum Surface Runoff Rate Kg/M2/S	24
4	5205	Convective Rainfall Rate Kg/M2/S	24
5	8225	Deep Soil Temp. After Hydrology Degk	24
6	3250	Dewpoint At 1.5M (K)	24
7	2207	Downward Lw Rad Flux: Surface	24
8	15214	Ertel Potential Vorticity Theta Surf	24
9	31	Frac Of Sea Ice In Sea After Tstep	24
10	16202	Geopotential Height On P Lev/P Grid	24
11	30	Land Mask (No Halo) (Land=True)	24
12	2201	Net Down Surface Lw Rad Flux	24
13	1201	Net Down Surface Sw Flux: SwTs Only	24
14	30208	Omega On P Lev/Uv Grid	24
15	33	Orography (/Strat Lower Bc)	24
16	2205	Outgoing Lw Rad Flux (Toa)	24
17	16222	Pressure At Mean Sea Level	24
18	23	Snow Amount Over Land Aft Tstp Kg/M2	24
19	8223	Soil Moisture Content In A Layer	24
20	30205	Specific Humidity On P Lev/Uv Grid	24
21	3234	Surface Latent Heat Flux W/M2	24
22	409	Surface Pressure After Timestep	24
23	3217	Surface Sensible Heat Flux W/M2	24
24	24	Surface Temperature After Timestep	24
25	3236	Temperature At 1.5M	24
26	30204	Temperature On P Lev/Uv Grid	24
27	9217	Total Cloud Amount Max/Random Overlp	24
28	30403	Total Column Dry Mass Rho Grid	24
29	30404	Total Column Wet Mass Rho Grid	24
30	1235	Total Downward Surface Sw Flux	24
31	5216	Total Precipitation Rate Kg/M2/S	6

32	5215	Total Snowfall Rate: Ls+Conv Kg/M2/S	24
33	30201	U Compnt Of Wind On P Lev/Uv Grid	24
34	30202	V Compnt Of Wind On P Lev/Uv Grid	24

Fields in file cplfca.pi20190501

Sl. No.	Stash Code	Field Name	Frequency
1	3329	1.5M Specific Humidity Over Tiles	24
2	3328	1.5M Temperature Over Tiles	24
3	3227	10 Metre Wind Speed On B Grid	24
4	3225	10 Metre Wind U-Comp B Grid	24
5	15212	50 Metre Wind U-Component B Grid	24
6	15213	50 Metre Wind V-Component B Grid	24
7	8233	Canopy Throughfall Rate Kg/M2/S	24
8	1210	Clear-Sky (Ii) Down Surface Sw Flux	24
9	1231	Diffuse Sw Flux On Levels	24
10	2207	Downward Lw Rad Flux: Surface	24
11	3297	Evap From Canopy : Rate Kg/M2/S	24
12	26002	Gridbox Outflow Kg/S	24
13	2201	Net Down Surface Lw Rad Flux	24
14	3291	Net Primary ProducPfts (Retd)	24
15	3262	Net Primary Productivity (Retd)	24
16	26001	River Water Storage Kg	24
17	23	Snow Amount Over Land Aft Tstp Kg/M2	24
18	8223	Soil Moisture Content In A Layer	24
19	3237	Specific Humidity At 1.5M	24
20	8235	Sub-Surface Runoff Rate Kg/M2/S	24
21	409	Surface Pressure After Timestep	24
22	8234	Surface Runoff Rate Kg/M2/S	24
23	5216	Total Precipitation Rate Kg/M2/S	1
24	5215	Total Snowfall Rate: Ls+Conv Kg/M2/S	24
25	3288	Transpiration+SoilEvp On Tiles	24
26	3463	Wind Gust	24

Fields in file cplfca.pm2019may

Sl. No.	Stash Code	Field Name	Frequency
1	3227	10 Metre Wind Speed On B Grid	m
2	3209	10 Metre Wind U-Comp	m
3	3225	10 Metre Wind U-Comp B Grid	m
4	3210	10 Metre Wind V-Comp	m
5	15212	50 Metre Wind U-Component B Grid	m
6	15213	50 Metre Wind V-Component B Grid	m
7	1210	Clear-Sky (Ii) Down Surface Sw Flux	m

8	31	Frac Of Sea Ice In Sea After Tstep	m
9	16202	Geopotential Height On P Lev/P Grid	m
10	30301	HeavysideFn On P Lev/Uv Grid	m
11	16222	Pressure At Mean Sea Level	m
12	8023	Snow Mass After Hydrology Kg/M2	m
13	8223	Soil Moisture Content In A Layer	m
14	30205	Specific Humidity On P Lev/Uv Grid	m
15	409	Surface Pressure After Timestep	m
16	24	Surface Temperature After Timestep	m
17	3236	Temperature At 1.5M	m
18	16203	Temperature On P Lev/P Grid	m
19	30204	Temperature On P Lev/Uv Grid	m
20	5216	Total Precipitation Rate Kg/M2/S	m
21	30201	U Compnt Of Wind On P Lev/Uv Grid	m
22	15201	U Wind On Pressure Levels B Grid	m
23	30202	V Compnt Of Wind On P Lev/Uv Grid	m
24	15202	V Wind On Pressure Levels B Grid	m

Fields in file cplfca.pt20190501

Sl. No.	Stash Code	Field Name	Frequency
1	3225	10 Metre Wind U-Comp B Grid	6
2	3226	10 Metre Wind V-Comp B Grid	6
3	8225	Deep Soil Temp. After Hydrology Degk	6
4	3250	Dewpoint At 1.5M (K)	6
5	2207	Downward Lw Rad Flux: Surface	24
6	31	Frac Of Sea Ice In Sea After Tstep	24
7	1207	Incoming Sw Rad Flux (Toa): All Tss	24
8	30	Land Mask (No Halo) (Land=True)	-
9	2201	Net Down Surface Lw Rad Flux	24
10	1201	Net Down Surface Sw Flux: SwTs Only	24
11	507	Open Sea Surface Temp After Timestep	6
12	33	Orography (/Strat Lower Bc)	-
13	1208	Outgoing Sw Rad Flux (Toa)	24
14	16222	Pressure At Mean Sea Level	6
15	508	Sea-Ice Surface Temp After Timestep	6
16	8223	Soil Moisture Content In A Layer	24
17	8235	Sub-Surface Runoff Rate Kg/M2/S	24
18	3234	Surface Latent Heat Flux W/M2	24
19	8234	Surface Runoff Rate Kg/M2/S	24
20	3217	Surface Sensible Heat Flux W/M2	24
21	3223	Surface Total Moisture Flux Kg/M2/S	24
22	3236	Temperature At 1.5M	24
23	3332	Toa Outgoing Lw Rad After B.Layer	24

24	9217	Total Cloud Amount Max/Random Overlp	6
25	1235	Total Downward Surface Sw Flux	24
26	5226	Total Precipitation Amount Kg/M2/Ts	24
27	5215	Total Snowfall Rate: Ls+Conv Kg/M2/S	24
28	3463	Wind Gust	24
29	3460	X-Comp Surface Bl Stress	24
30	3461	Y-Comp Surface Bl Stress	24

Fields in file cplfca.pu20190501

Sl. No.	Stash Code	Field Name	Frequency
1	16202	Geopotential Height On P Lev/P Grid	12
2	30205	Specific Humidity On P Lev/Uv Grid	12
3	16203	Temperature On P Lev/P Grid	12
4	15201	U Wind On Pressure Levels B Grid	12
5	15202	V Wind On Pressure Levels B Grid	12

Appendix B.2: List of output ocean variables

Fields in file cplhco_1d_20151101_20151207_grid_T.nc

Sl. No.	Field Name	Units	Frequency
1	Ice Concentration	%	1D
2	Ice Meridional Current	m/s	1D
3	Ice Zonal Current	m/s	1D
4	Ocean Mixed Layer Thickness Defined By Sigma Theta	m	1D
5	Sea Surface Height Above Geoid	m	1D
6	Sea Water Potential Temperature	C	1D
7	Sea Water Salinity	PSU	1D

Fields in file cplhco_1d_20151101_20151207_grid_U.nc

Sl. No.	Field Name	Units	Frequency
1	Sea Water X Velocity	m/s	1D

Fields in file cplhco_1d_20151101_20151207_grid_V.nc

Sl. No.	Field Name	Units	Frequency
1	Sea Water Y Velocity	m/s	1D

Fields in file cplhco_1d_20151101_20151207_grid_W.nc

Sl. No.	Field Name	Units	Frequency
1	Upward Sea Water Velocity	m/s	1D

Fields in file cplhco_1m_20151101_20151130_grid_T.nc

Sl. No.	Field Name	Units	Frequency
1	Downwelling Photosynthetic Radiative Flux In Sea Water	W/m2	1M
2	Ice Concentration	%	1M
3	Ice Meridional Current	m/s	1M
4	Ice Zonal Current	m/s	1M
5	Ocean Mixed Layer Thickness Defined By Sigma Theta	m	1M
6	Sea Surface Height Above Geoid	m	1M
7	Sea Water Potential Temperature	C	1M
8	Sea Water Potential Temperature At Sea Floor	C	1M
9	Sea Water Salinity	PSU	1M
10	Snow Thickness (Cell Average)	m	1M
11	Surface Downward Heat Flux In Sea Water	W/m2	1M
12	Water Flux Out Of Sea Ice And Sea Water	kg/m2/s	1M

Fields in file cplhco_1m_20151101_20151130_grid_U.nc

Sl. No.	Field Name	Units	Frequency
1	Sea Water X Velocity	m/s	1M
2	Surface Downward X Stress	N/m2	1M

Fields in file cplhco_1m_20151101_20151130_grid_V.nc

Sl. No.	Field Name	Units	Frequency
1	Sea Water Y Velocity	m/s	1M
2	Surface Downward Y Stress	N/m2	1M

Fields in file cplhco_1m_20151101_20151130_grid_W.nc

Sl. No.	Field Name	Units	Frequency
1	Upward Sea Water Velocity	m/s	1M

Appendix B.3: List of output seaice variables

Fields in file cplhci_1d_20151101_20151207_grid_I.nc

Sl. No.	Field Name	Units	Frequency
1	Grid Cell Mean Ice Thickness	m	1D
2	Heat Flux Ice To Ocean	W/m^2	1D
3	Ice Area (Aggregate)	1	1D
4	Ice Velocity (X)	m/s	1D
5	Ice Velocity (Y)	m/s	1D
6	Ice Volume, Categories	m	1D
7	Net Surface Heat Flux	W/m^2	1D
8	Ocean Current (X)	m/s	1D
9	Ocean Current (Y)	m/s	1D
10	Sea Surface Salinity	ppt	1D
11	Sea Surface Temperature	C	1D

Fields in file cplhci_1m_20151101_20151130_grid_I.nc

Sl. No.	Field Name	Units	Frequency
1	Area Tendency Dynamics	%/day	1M
2	Area Tendency Thermo	%/day	1M
3	Atm/Ice Stress (X)	N/m^2	1M
4	Atm/Ice Stress (Y)	N/m^2	1M
5	Basal Ice Melt	cm/day	1M
6	Compressive Ice Strength	N/m	1M
7	Congelation Ice Growth	cm/day	1M
8	Coriolis Stress (X)	N/m^2	1M
9	Coriolis Stress (Y)	N/m^2	1M
10	Evaporative Water Flux	cm/day	1M
11	Fraction Of Time-Avg Interval That Ice Is Present	1	1M
12	Frazil Ice Growth	cm/day	1M
13	Freeze Onset Date	day of year	1M
14	Freeze/Melt Potential	W/m^2	1M
15	FreshwtrFlx Ice To Ocn	cm/day	1M
16	Grid Cell Mean Ice Thickness	m	1M
17	Grid Cell Mean Snow Thickness	m	1M
18	Heat Flux Ice To Ocean	W/m^2	1M
19	Ice Area (Aggregate)	1	1M
20	Ice Area Ridging Rate	%/day	1M
21	Ice Area, Categories	1	1M
22	Ice Velocity (X)	m/s	1M
23	Ice Velocity (Y)	m/s	1M

24	Ice Volume Ridging Rate	cm/day	1M
25	Ice Volume, Categories	m	1M
26	Internal Ice Stress (X)	N/m^2	1M
27	Internal Ice Stress (Y)	N/m^2	1M
28	Internal Stress Tensor Trace	N/m^2	1M
29	Latent Heat Flux	W/m^2	1M
30	Latent Heat Flux, Category	W/m^2	1M
31	Lateral Ice Melt	cm/day	1M
32	Lead Area Opening Rate	%/day	1M
33	Melt Onset Date	day of year	1M
34	Net Sfc Heat Flux Causing Melt, Cat	W/m^2	1M
35	Net Surface Heat Flux	W/m^2	1M
36	Net Surface Heat Flux Causing Melt	W/m^2	1M
37	Net Surface Heat Flux, Categories	W/m^2	1M
38	Norm. Principal Stress 1	1	1M
39	Norm. Principal Stress 2	1	1M
40	Ocean Current (X)	m/s	1M
41	Ocean Current (Y)	m/s	1M
42	Ocean/Ice Stress (X)	N/m^2	1M
43	Ocean/Ice Stress (Y)	N/m^2	1M
44	Rainfall Rate	cm/day	1M
45	Ridge Area Formation Rate	%/day	1M
46	Salt Flux Ice To Ocean	kg/m^2/s	1M
47	Sea Surface Salinity	ppt	1M
48	Sea Surface Temperature	C	1M
49	Snow-Ice Formation	cm/day	1M
50	Snowfall Rate	cm/day	1M
51	Strain Rate (Divergence)	%/day	1M
52	Strain Rate (Shear)	%/day	1M
53	Sw Flux Thru Ice To Ocean	W/m^2	1M
54	Top Ice Melt	cm/day	1M
55	Top Sfc Conductive Heat Flux, Cat	W/m^2	1M
56	Top Snow Melt	cm/day	1M
57	Top Surface Conductive Heat Flux	W/m^2	1M
58	Volume Tendency Dynamics	cm/day	1M
59	Volume Tendency Thermo	cm/day	1M

Appendix C: Model output fields only available in forecasts

Fields in file cplfco_12h_20190501_20190508_grid_T.nc

Sl. No.	Field Name	Units	Frequency
1	Ice Concentration	%	12H
2	Ice Thickness (Cell Average)	m	12H
3	In-Situ Temperature	C	12H
4	Ocean Mixed Layer Thickness Defined By Sigma Theta	m	12H
5	Sea Surface Height Above Geoid	m	12H
6	Sea Water Potential Temperature	C	12H
7	Sea Water Salinity	PSU	12H
8	Snow Thickness (Cell Average)	m	12H

Fields in file cplfco_12h_20190501_20190508_grid_U.nc

Sl. No.	Field Name	Units	Frequency
1	Sea Water X Velocity	m/s	12H

Fields in file cplfco_12h_20190501_20190508_grid_V.nc

Sl. No.	Field Name	Units	Frequency
1	Sea Water Y Velocity	m/s	12H

Fields in file cplfco_1d_20190501_20190508_grid_T.nc

Sl. No.	Field Name	Units	Frequency
1	Downwelling Photosynthetic Radiative Flux In Sea Water	W/m2	1D
2	Ice Concentration	%	1D
3	Ice Meridional Current	m/s	1D
4	Ice Zonal Current	m/s	1D
5	Ocean Mixed Layer Thickness Defined By Sigma Theta	m	1D
6	Sea Surface Height Above Geoid	m	1D
7	Sea Water Potential Temperature	C	1D
8	Sea Water Potential Temperature At Sea Floor	C	1D
9	Sea Water Salinity	PSU	1D
10	Snow Thickness (Cell Average)	m	1D
11	Surface Downward Heat Flux In Sea Water	W/m2	1D
12	Water Flux Out Of Sea Ice And Sea Water	kg/m2/s	1D

Fields in file cplfco_1d_20190501_20190508_grid_U.nc

Sl. No.	Field Name	Units	Frequency
1	Sea Water X Velocity	m/s	1D
2	Surface Downward X Stress	N/m2	1D

Fields in file cplfco_1d_20190501_20190508_grid_V.nc

Sl. No.	Field Name	Units	Frequency
1	Sea Water Y Velocity	m/s	1D
2	Surface Downward Y Stress	N/m2	1D

Fields in file cplfco_1d_20190501_20190508_grid_W.nc

Sl. No.	Field Name	Units	Frequency
1	Upward Sea Water Velocity	m/s	1D

Fields in file cplfco_3h_20190501_20190508_grid_T.nc

Sl. No.	Field Name	Units	Frequency
1	Ice Concentration	%	3H
2	Ice Thickness (Cell Average)	m	3H
3	Ocean Mixed Layer Thickness Defined By Sigma Theta	m	3H
4	Sea Surface Height Above Geoid	m	3H
5	Sea Surface Salinity	PSU	3H
6	Sea Surface Temperature	C	3H

Fields in file cplfco_3h_20190501_20190508_grid_U.nc

Sl. No.	Field Name	Units	Frequency
1	Ocean Current Along I-Axis: Surface	m/s	3H

Fields in file cplfco_3h_20190501_20190508_grid_V.nc

Sl. No.	Field Name	Units	Frequency
1	Ocean Current Along J-Axis: Surface	m/s	3H

Fields in file cplfci_1d_20190501_20190508_grid_I.nc

Sl. No.	Field Name	Units	Frequency
1	Area Tendency Dynamics	%/day	1D
2	Area Tendency Thermo	%/day	1D
3	Atm/Ice Stress (X)	N/m^2	1D
4	Atm/Ice Stress (Y)	N/m^2	1D
5	Basal Ice Melt	cm/day	1D
6	Compressive Ice Strength	N/m	1D
7	Congelation Ice Growth	cm/day	1D
8	Coriolis Stress (X)	N/m^2	1D
9	Coriolis Stress (Y)	N/m^2	1D
10	Evaporative Water Flux	cm/day	1D
11	Fraction Of Time-Avg Interval That Ice Is Present	1	1D
12	Frazil Ice Growth	cm/day	1D
13	Freeze Onset Date	day of year	1D
14	Freeze/Melt Potential	W/m^2	1D
15	FreshwtrFlx Ice To Ocn	cm/day	1D
16	Grid Cell Mean Ice Thickness	m	1D
17	Grid Cell Mean Snow Thickness	m	1D
18	Heat Flux Ice To Ocean	W/m^2	1D
19	Ice Area (Aggregate)	1	1D
20	Ice Area Ridging Rate	%/day	1D
21	Ice Area, Categories	1	1D
22	Ice Velocity (X)	m/s	1D
23	Ice Velocity (Y)	m/s	1D
24	Ice Volume Ridging Rate	cm/day	1D
25	Ice Volume, Categories	m	1D
26	Internal Ice Stress (X)	N/m^2	1D
27	Internal Ice Stress (Y)	N/m^2	1D
28	Internal Stress Tensor Trace	N/m^2	1D
29	Latent Heat Flux	W/m^2	1D
30	Latent Heat Flux, Category	W/m^2	1D
31	Lateral Ice Melt	cm/day	1D
32	Lead Area Opening Rate	%/day	1D
33	Melt Onset Date	day of year	1D
34	Net Sfc Heat Flux Causing Melt, Cat	W/m^2	1D
35	Net Surface Heat Flux	W/m^2	1D
36	Net Surface Heat Flux Causing Melt	W/m^2	1D
37	Net Surface Heat Flux, Categories	W/m^2	1D
38	Norm. Principal Stress 1	1	1D
39	Norm. Principal Stress 2	1	1D

40	Ocean Current (X)	m/s	1D
41	Ocean Current (Y)	m/s	1D
42	Ocean/Ice Stress (X)	N/m^2	1D
43	Ocean/Ice Stress (Y)	N/m^2	1D
44	Rainfall Rate	cm/day	1D
45	Ridge Area Formation Rate	%/day	1D
46	Salt Flux Ice To Ocean	kg/m^2/s	1D
47	Sea Surface Salinity	ppt	1D
48	Sea Surface Temperature	C	1D
49	Snow-Ice Formation	cm/day	1D
50	Snowfall Rate	cm/day	1D
51	Strain Rate (Divergence)	%/day	1D
52	Strain Rate (Shear)	%/day	1D
53	Sw Flux Thru Ice To Ocean	W/m^2	1D
54	Top Ice Melt	cm/day	1D
55	Top Sfc Conductive Heat Flux, Cat	W/m^2	1D
56	Top Snow Melt	cm/day	1D
57	Top Surface Conductive Heat Flux	W/m^2	1D
58	Volume Tendency Dynamics	cm/day	1D
59	Volume Tendency Thermo	cm/day	1D